Carbonization of Saccharide-based Materials for Wastewater Treatment Applications

Edith Odinaka Ahaka

Submitted to the
Institute of Graduate Studies and Research
in partial fulfillment of the requirements for the degree of

Doctor of Philosophy
in
Chemistry

Eastern Mediterranean University
November 2019
Gazimağusa, North Cyprus

Approval of the Institute of Graduate Studies and Research

Prof. Dr. Ali Hakan Ulusoy
Acting Director

I certify that this thesis satisfies all the requirements as a thesis for the degree of Doctor of Philosophy in Chemistry.

Prof. Dr. İzzet Sakallı
Chair, Department of Chemistry

We certify that we have read this thesis and that in our opinion it is fully adequate in scopeand quality as a thesis for the degree of Doctor of Philosophy in Chemistry.

Assoc. Prof. Dr. Akeem Oladipo
Co-Supervisor

Prof. Dr. Mustafa Gazi
Supervisor

Examining Committee

1. Prof. Dr. Mustafa Gazi
2. Prof. Dr. Bahire Filiz Şenkal
3. Prof. Dr. Zehra Tuba Şişmanoğlu
4. Prof. Dr. Elvan Yılmaz
5. Assoc. Prof. Dr. Hayrettin Ozan Gülcan

ABSTRACT

Carbonized saccharide-based materials have potentials to be effectively used for the purification of wastewater. Saccharide-based materials are rich carbon-based materials, and herein banana peels and discarded chewing gum was exploited. Pyrochar/AgBr derived from discarded chewing gum was used for the decontamination of trichlorophenol (2,4,5-TCP) while biochar derived from banana peel waste was effectively used for the elimination of heavy metals ions. The surface, morphology, and magnetic properties of the prepared adsorbents were examined by Boehm titration; Fourier-transform infrared techniques and scanning electron microscope. The adsorption isotherm and kinetic behaviour of the pollutants were examined, and the results comprehensively explained.

The pyrochar/AgBr possesses a pore volume and a S_{BET} of 0.998 cm^3/g and 249.5 m^2/g respectively. 2,4,5-TCP removal efficiency at 10 mg/L was estimated to be ~96% and the Yoon–Nelson and Thomas models successfully described its dynamic behaviour. For the first time, commonly discarded chewing gum was employed as a prototype for the fabrication of high performing adsorbents engaged for the treatment of wastewater**.** Desorption and re-usability of pyrochar/AgBr were also assessed.

The magnetic calcined biochar (MCB) possesses a high saturation magnetization value at 39.55 emu/g, porous structures, surface functional groups (COO^- and–OH), and an S_{BET} larger than the (CB). The optimum adsorption capacity of MCB at pH 6 are 72.8, 75.9, and 83.4 mg/g for Zn^{2+}, Cu^{2+}, and Hg^{2+}, respectively for the single-component adsorption and suitably fits in the Langmuir and Redlich-Peterson

adsorption isotherms and the pseudo-second order for the adsorption kinetic models. MCB exhibited higher adsorption affinity toward Hg^{2+} than Cu^{2+} and Zn^{2+} for the multicomponent system as shown in the extended Langmuir isotherm (selectivity factor values).

Keywords: Biochar; Discarded chewing gum; Banana peel; Magnetic biochar; trichlorophenol decontamination; heavy metals; Adsorption

ÖZ

Kömürleşmiş sakkarit bazlı malzemeler, atık suyun arıtılmasında etkin bir şekilde kullanılma potansiyeline sahiptir. Sakkarit bazlı malzemeler, zengin karbon bazlı malzemeler olup bu çalışmada muz kabukları ve atık sakızlar kullanılmıştır. Atık sakızlardan elde edilen Pyrochar / AgBr, triklorofenolun (2,4,5-TCP) dekontaminasyonu için kullanılırken, muz kabuğu atıklarından üretilen biyokömür (biochar), ağır metal iyonlarının giderilmesi için etkili bir şekilde kullanıldı. Hazırlanan adsorbent malzemelerin yüzey, morfoloji ve manyetik özellikleri Boehm titrasyonu; Fourier dönüşümü kızılötesi teknikleri ve taramalı elektron mikroskobu ile incelendi. Kirleticilerin adsorpsiyon izotermi ve kinetik davranışı incelenmiş ve sonuçlar kapsamlı bir şekilde açıklanmıştır.

Biyokömür (Pyrochar) / AgBr' ın gözenek hacmi ve S_{BET} ' I sırası ile 0.998 cm^3 / g ve 249.5 m^2/g olarak bulunmuştur. 2,4,5-TCP'nin 10 mg/L'deki TCP giderimi veriminin ~% 96 olduğu bulundu ve Yoon-Nelson ve Thomas modelleri dinamik davranışını başarılı bir şekilde açıkladı. İlk kez, atık sakız, kirli suyun arıtılması için çalışılan yüksek performanslı adsorbanların imalatı için bir prototip olarak kullanılmıştır. Pyrochar / AgBr'nin desorpsiyonu ve yeniden kullanılabilirliği de değerlendirildi.

Manyetik kalsine biochar (MCB) 39.55 emu/g'de yüksek doygunlukta bir mıknatıslanma değerine, gözenekli yapılara, yüzey fonksiyonel gruplarına (COO− ve-OH) ve (CB) 'den daha büyük bir S_{BET}'e sahiptir. MCB'nin pH 6'da optimum adsorpsiyon kapasitesi, Zn^{2+}, Cu^{2+} ve Hg^{2+} için sırasıyla 72.8, 75.9 ve 83.4 mg /

g'dir, Langmuir ve Redlich-Peterson adsorpsiyon izotermlerine ve yalancı ikinci derece adsorpsiyon kinetiği modellerine uyar. MCB, genişletilmiş Langmuir izoterminde (seçicilik faktörü değerleri) gösterildiği gibi çok bileşenli sistem için Hg^{2+}'ya Cu^{2+} ve Zn^{2+}'dan daha yüksek adsorpsiyon afinitesi göstermiştir.

Anahtar Kelimeler: Biyokömür; Atık sakız; Muz kabuğu; Manyetik biyokömür; triklorofenol dekontaminasyonu; ağır metaller; adsorpsiyon

DEDICATION

This thesis is dedicated to the way-maker, ever faithful God, lover of my soul, my beautifier in whom I live, move and have my being.

ACKNOWLEDGEMENT

First and foremost, my indebt grateful is to God for the breath of life, ability, and sufficient grace lavished on me to bring this work to completion. For the light that shone in my dark times, encouragements in my seasons of discouragements and His hand that held me through.

A profound appreciation to my Prof. Dr. Mustafa Gazi, PhD thesis supervisor for the assistance rendered throughout the process of this thesis. I could not neglect the immeasurable input of the co-supervisor of my work, Assoc. Prof. Dr. Akeem Oladipo, who gave his every all for this work to get to this point. A deep-seated thanks to him for his patience to put me through and his immeasurable contribution every step of the way.

To my wonderful colleagues, Ayodeji Ifebajo, Anthony Awode, Kola Azalok, and everyone, a big thanks for your support and presence which were always a big encouragement for me. To the wonderful friends I was opportuned to meet in the course of my sojourn, Bethesda church (family of love), my sweet sister Miracle Iruke who were with me all through and were unfainting in their prayers for me, God bless you richly. Thank you for everything Serap Sunal, manager, Sabanci dormitory, you made living easy for me.

My indebt thanks to my loving and understanding husband, Mr. Matthew Agboola, it wasn't easy but you let me pursue this to the very end and still gave me the push I needed in all wise. I owe it to my family especially my lovely parents who ensured that I never gave up hope and supported me to the last of it.

TABLE OF CONTENTS

LIST OF TABLES

LIST OF FIGURES

LIST OF SYMBOLS AND ABBREVIATIONS

2,4,5-TCP	2,4,5-Trichlorphenol
ARE	Average Relation Error
ARS	Average Relation Standard Error
BET	Brunauer-Emmett-Teller
CB	Calcined Biochar
C_e	Concentration at equilibrium (mg/L)
C_i	Influent concentration (mg/L)
EDX	Energy Dispersed X-ray Spectroscopy
F	Flow rate (mL/min)
K_{TH}	Thomas Rate Constant ($mLmg^{-1}min^{-1}$)
K_{YN}	Rate Constant (min^{-1})
MCB	Magnetic Calcined Biochar
q_e	Equilibrium Adsorption Efficiency (mg/g)
q_m or q_{TH}	Maximum Adsorption Efficiency (mg/g)
R^2	Correlation Coefficient Value
t_b	Breakthrough time (min)
t_e	Exhaustion time (min)
XRD	X-ray Diffraction
Z	Bed height (cm)
λ_{max}	Maximum Wavelength
τ	50% adsorbate breakthrough time (min)
χ	Relative Low Error

Chapter 1

INTRODUCTION

Environmental issues arising from pollution by wastewater is increasingly alarming recently. Particularly, the wastewater originating from process industries generally contain various organic and inorganic contaminants which include toxic dyes, heavy metals (Barakat, 2011; Farooq et al., 2010; Oladipo & Gazi, 2015a). Also, phenol and the phenolic derivatives are unsafe pollutants generated in wood, oil refinery, pharmaceuticals and olive-based industries (Blackburn, 2004; Crini, 2005). The presence of these pollutants in the aquatic environs is consequently detrimental to living organisms.

Notably, phenols and derivatives of phenols have increased resistance to biological decomposition due to the presence of a benzene ring that is stable in their structure (Mohammadi et al., 2015). The recent trend in research centres on the elimination of chlorophenols (a suspicious carcinogen) from wastewater, a consequential effect of the discharge of phenols into the aquatic habitat. They are also introduced into the environment from resultant activities of pharmaceutical and chemical industries. There have been several attempts to eliminate these compounds from water and resolve this problem using different treatment methods (Busca et al., 2008; Villegas et al., 2016). The common treatment technique is adsorption and advanced oxidation processes (AOPs) (Singh & Arora, 2011). Interestingly, the AOPs are regarded as the highly effective technologies for achieving the maximum limits of phenol allowed.

Notwithstanding, these processes are relatively expensive and may require complex equipment and selective catalysts (Ahmed et al., 2011).

The choice of adsorption processes as an adequate method for the treatment of wastewater has become prevalent in recent times, by virtue of its simplicity, convenient unit operation and low cost which distinguish it from other treatment methods. Activated carbon, which possesses a removal capacity that is high due to its large surface area, has been greatly recognized as an effective adsorbent. But these activated carbons as adsorbents have limitations which spring from their high cost and difficulties in been recovered from treated water (Bhatnagar et al., 2015). The application of waste biomass or spent saccharide based materials which are widely available as well as low cost adsorbents provides a creative and alluring alternative (De Gisi et al, 2016).

Saccharides are organic compounds comprising of carbon, hydrogen, and oxygen elemental atoms at proportions of 1, 2, and 1 respectively, having an empirical formula of $C_x(H_2O)_y$. They are carbon-rich and easily accessible as such it's suitable as low-cost adsorbents. Saccharides are also known as sugars molecules and are classified based on the number of sugar molecules they possess i.e. monosaccharide (simple sugars), disaccharide, oligosaccharide and polysaccharide. They originate from plant foods like cereals, fruits, legumes, root vegetables and are also added to foods such as dairy products, juices, jams, soft drinks, energy drinks, liqueurs, and sweets (Blackburn, 2004; Crini, 2005)

Carbonization is the alteration of a material into a carbon-rich residue by way of pyrolysis. Carbonization process can be performed via dry pyrolysis or wet pyrolysis

(hydrothermal carbonization). The dry process requires the biomass to be relatively dry before conversion and it is done at high temperatures and inert atmosphere, while the hydrothermal process starts with biomass in its original form and it is done at temperatures between 180^{o}C and 250^{o}C under autogenous pressures (Lucian & Fiori, 2017). Herein, research focus is directed towards the carbonization of different readily available saccharides. The carbonized products and composite are then used as adsorbents and efficient catalysts for the ejection of various inorganic and organic impurities from wastewaters.

1.1 Objectives of this thesis

The sole purpose of this work is the production of low-cost alternative carbonized adsorbents which are reusable and environmentally stable for efficient adsorptive elimination of heavy metals and pesticides from wastewater. Specific goals include:

- Production of economical but high performance carbonized adsorbents
- Modification of the carbonized materials produced for better enhanced elimination of inorganic and organic contaminants
- To efficiently model the treatment factors and obtain the optimal operating conditions
- To build the mechanism of removal of the studied pollutants using the prepared composites

1.2 Scope of this study

This thesis centers on the preparation of carbonized materials from saccharide-based (often locally available) materials employed to eliminate heavy metals (mercury, copper, and zinc in this study) and pesticides (2,4,5-trichlorophenol) from wastewater. The wastewater was artificially simulated in the laboratory. The

adsorbents and their modified derivatives were tested for their efficiencies in removing the aforementioned pollutants for both batch and fix-bed studies.

The synthesized adsorbents were intensively characterized, and the analyte concentrations were determined using UV─VIS spectrophotometer (Beijing, T80+) under ambient conditions. The adsorption procedures were run in triplicates and the average value of results were noted for all stages to obtain stability of the results. Fixed-bed adsorption process was done in a column loaded with wool at both layers in similar conditions with batch studies. The criteria investigated were optimized to obtain the highest removal efficiency. Also, regeneration and reusability of spent of adsorbents were assessed. Various adsorption kinetics and isotherms of adsorption were adapted to analyze the mechanism of removal.

1.3 Structure of the thesis

This whole report has been categorized as thus:

Chapter One establishes the problem statement, the need, the scope and objective of this research

Chapter Two surveys studies reported by other researchers. It is explicit on carbonization, the need for the preference of adsorption technique for elimination of impurities and the adoption of low-cost adsorbents.

Chapter Three reviews the experimental methods used to accomplish the desired objectives. It outlines the adsorbent and chemical materials used, tests performed, equipment used, and appropriate information about the experiments.

Chapter Four explains the results obtained from the experiments. It also explains the sequence of events observed during the experiments. Here, the optimum conditions of operation were also featured.

Chapter Five gives a comprehensive conclusion of the accrued results obtained from this work as well as propositions.

Chapter 2

LITERATURE REVIEW

2.1 General Information

Water as an imperative necessity to all aspects of human life cannot be overlooked. A British Poet, W. H. Auden had stated that "Thousands can live without love, not one has ever lived without water." It's pathetic how the importance of safe water is trashed as our water bodies are continually polluted with mostly untreated wastewater. Water is necessary for our economy, food, energy and health (Amin et al., 2014) as such the need for wastewater treatment applications to ensure safe water resources. Water treatment aims at getting rid of undesired impurities which are toxic and harmful and restoring the water quality to meet the requirements of current stringent regulations (Malik, 2004; Reungoat et al., 2012). The impurities in wastewater can be categorized into plant nutrients, integrated and non-integrated substances, heavy metals, and organic substances (Reungoat et al., 2012).

2.2 Pollutants in Wastewater Effluents

Daily, wastewater effluents comprising of pollutants are generated from industrial and even domestic activities. Amidst all liquids, water has a greatest ability to readily dissolve substance hence called a "universal solvent". These pollutants consequently jeopardize our health. Water pollutants (contaminants) are harmful, unhealthy, unsafe and toxic substances that contaminate water bodies. Water contaminants can be categorized majorly as indicated in Figure 1. This research centered on the eradication of pesticides and heavy metals from wastewater effluents.

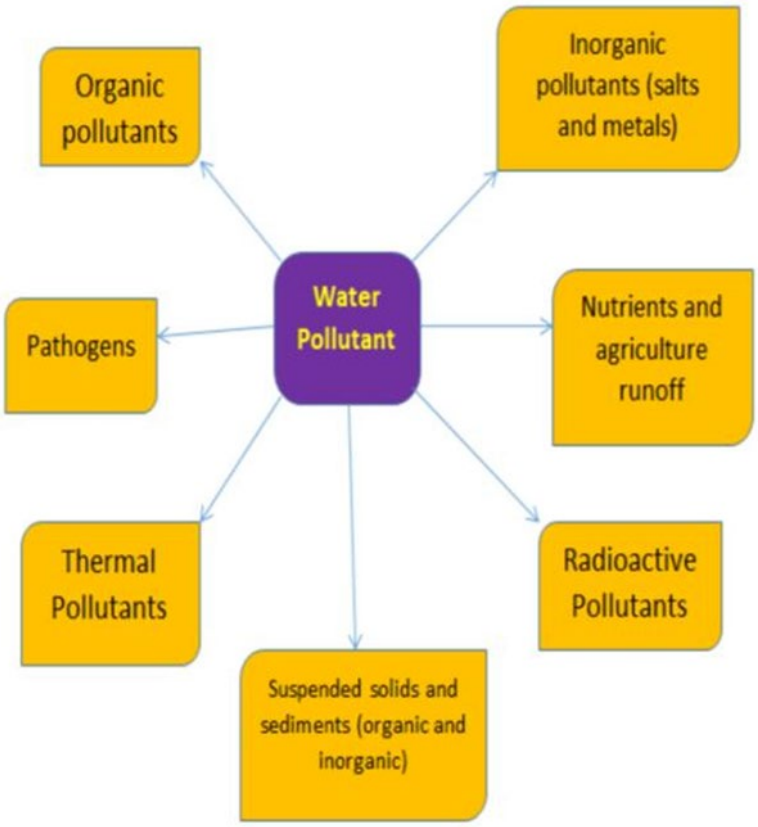

Figure 1: Categories of Water Pollutants

2.2.1 Pesticides

Pesticides are a class of organic pollutants and can also be gotten from the agricultural runoff. They are designed to protect agricultural products from the infestation of pests but their residues flow into water bodies through wastewater effluents and surface runoffs (Munze et al., 2017). Pesticides and plant growth stimulators are agrochemicals applied increasingly to agricultural lands to meet the fast-growing food demand globally. Pesticides constitute essential aspects of modern agriculture, essentially, to prevent disease (insecticides/fungicides) spread and weeds infestation (weedicides/herbicides). However, their persistent and excessive application results in soil pollution, farmland damage; and deteriorated environment and soil quality. Note that pesticides often accumulate in the environment (for many years) because they are persistent and recalcitrant pollutants.

Chemicals used to destroy or control pests are inclusive in the term pesticides. Pesticides are classified based on their origin and based on the types as shown in Figure 2. The impact of pesticides in wastewater effluents depends on the products of degradation, toxic effect, the measure of half-life (persistence), and environmental behaviour. Pesticides in water consequently produce detrimental health effects on human beings as well as on animals which comprise.

- Interruption of the hormonal system
- Cancers, tumors and lesions.
- Reproductive inhibition or failure.
- Weakening of the immune system.
- Cellular and DNA damage.
- Death

The list of examples of pesticides are endless, some are DDT, boric Acid, diazinon, chlorpyrifos, chlorophenol, nitrophenol, chlordane, toxaphene, oxasulfuron, nicosulfuron, glyphosate, acephate, deet, amidosulfuron, atrazine, Cyhexatin, Chlordimeform, Dieldrin etc. Majority of the chemical pesticides are retained within the body of organisms because they are fat-soluble. The absorbed pesticides can mimic the hormones and long term exposure results in the adverse effects listed above.

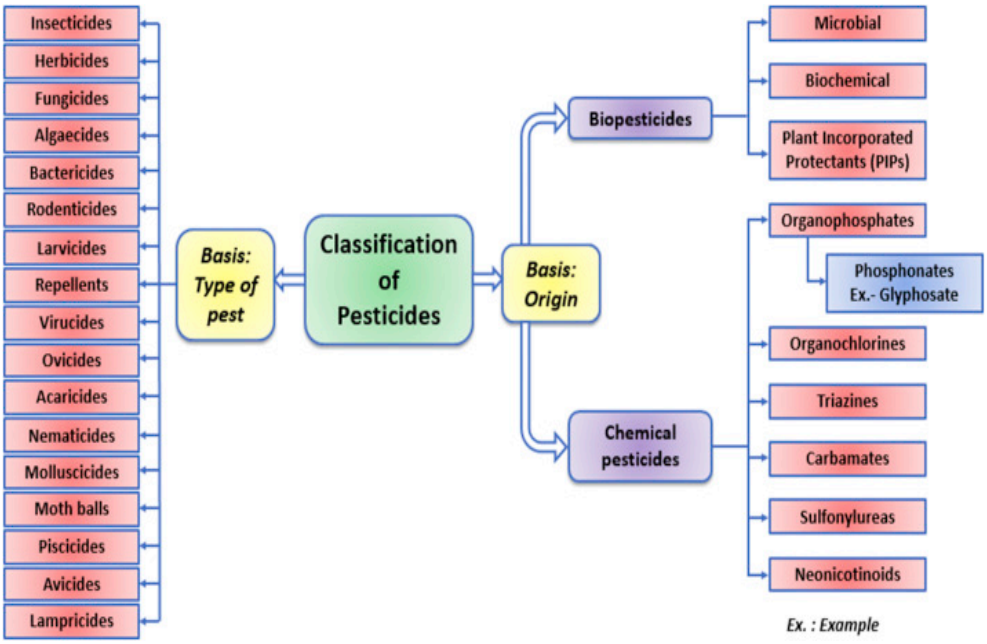

Figure 2: Categories of Pesticides (Oladipo et al., 2019)

Considering the negative impacts of excess pesticides in water bodies, air and soil; researchers have adopted various remediation technologies (chemical, physical, biological or hybrid) to eliminate or reduce these pesticides. Remediation of pesticides can be achieved by any of the commonly used techniques for other persistent and emerging organic pollutants with similar characteristics. The commonly used remediation technologies are separation (adsorption), immobilization and destruction (chemical and biological) technologies.

2.2.2 Heavy metals

These are classified under the "inorganic pollutants" category. Heavy metals are trace elements having atomic densities more than 4 g cm^{-3} and said to be highly toxic even at small concentrations (Pugazhenthiran et al., 2016). They belong to the group of metalloids and metals i.e. silver (Ag), mercury (Hg), lead (Pb), cadmium (Cd), iron (Fe), chromium(Cr), zinc (Zn), mercury (Hg), arsenic (As), copper (Cu), and arsenic (As) (Akpor et al., 2014; Barakat, 2011). The existence of these metals in the aquatic habitat causes crucial upsurge in the environment and health problems

(Oladipo & Gazi, 2015a). Table 1 outlines various metal toxicities and their maximum contaminant level according to USEPA (United State Environmental Protection Agency). The release of heavy metals into water bodies occurs majorly via natural and human activities;

- Natural pathways: i.e. volcanic eruptions, soil erosion, leaching of rocks, air contamination (aerosol particles)
- Human pathways: i.e. metal finishing, textile industries, electroplating processes, mining extraction operations, combustion processes and nuclear power

Table 1: The toxicities, standards and sources of heavy metals (Barakat, 2011; Farooq et al., 2010)

Heavy Metals	Toxicities	Maximum Contaminant Level (mg/L) according to USEPA	Sources
Copper	Insomnia, liver damage, reproductive and developmental toxicity, Wilson disease, and diarrhoea.	0.25	Wood preservatives, electroplating, paint production, copper mining & polishing, printing activities.
Zinc	Depression, neurological signs, lethargy, nausea, and gastrointestinal stress.	0.80	Manufacturing and mining activities.
Mercury	Kidney disease, rheumatoid arthritis, and nervous and circulatory system breakdown	0.00003	Volcanic eruptions, metallurgical and mining processes, paint production, forest fires, batteries, biogenic emissions, and weathering of mercury – containing areas.
Chromium	Carcinogenic, headache, nausea, vomiting, severe diarrhea, and lung tumors.	0.05	Metal processing, leather tanning, electroplating, paints, textile, and wood preservatives,
Nickel	Chronic bronchitis, chronic asthma, nausea, lung cancer and coughing.	0.2	Electroplating, mineral processing, porcelain enameling, and paint formulation.
Lead	Diminishing IQ, anaemia, anorexia, loss of appetite, brain damage, nervous and circulatory system.	0.006	Paints and pigments, Electroplating, ammunitions, and production of batteries.

2.3 Methods of Wastewater Treatment

Critical interest on adequate methods for the eradication of undesired compounds from wastewater is of paramount importance. The method used for the wastewater treatment is determined by the character of the wastewater. The methods of wastewater treatment can be broadly categorized as illustrated in Figure 3 below

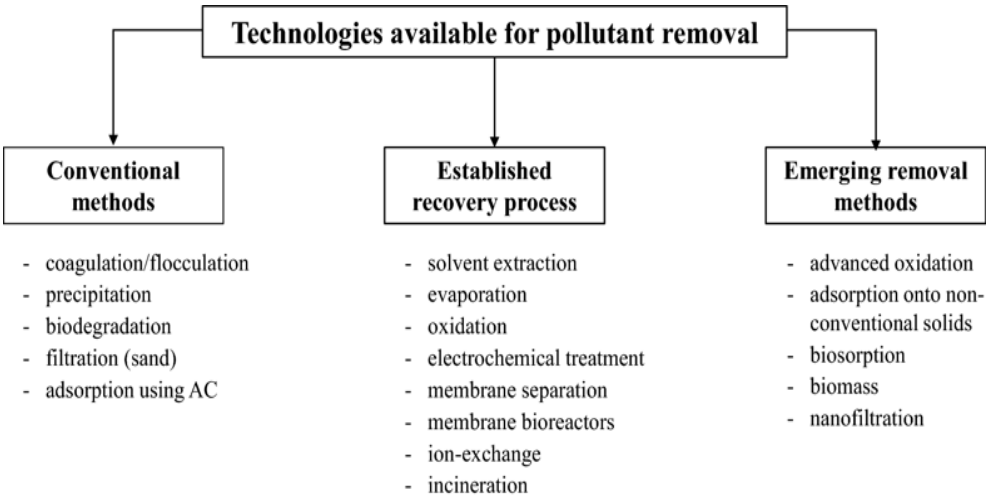

Figure 3: Broad overview of wastewater treatment technologies (Crini & Lichtfouse, 2019)

2.3.1 Coagulation and Flocculation method

These are techniques considered alongside each other used in the treatment of wastewater as well as in food industries, biochemistry, cosmetics, rubber manufacturing, paper and pulp, pharmaceutical, textiles, etc. They are employed for the removal of particles termed colloids which are usually less than 1 μm in size and cannot be probably removed only by filtration or sedimentation (Rossini et al., 1999). These particles have insufficient settling characteristics and are responsible for the turbidity and colour changes of water. Examples include micro-organisms, clays, protein metal oxides, and organic substances. Their poor aggregation and settling ability results from the negative charge they possess alongside the interaction between the colloids and water. The removal mechanism results from the

counteraction of the colloids that are negatively charged colloids (coagulants as illustrated in Figure 4) which allows for the initial collection (coagulation) of the fragments to form microfloc enhanced by the Van der Waals forces of attraction. Efficiency of these coagulation-flocculation processes are determined by temperature, coagulant type, pH, effluent quality, the distribution of colloidal particles in suspensions dosage, total dissolved solids, and ionic strength (Sher et al., 2013).

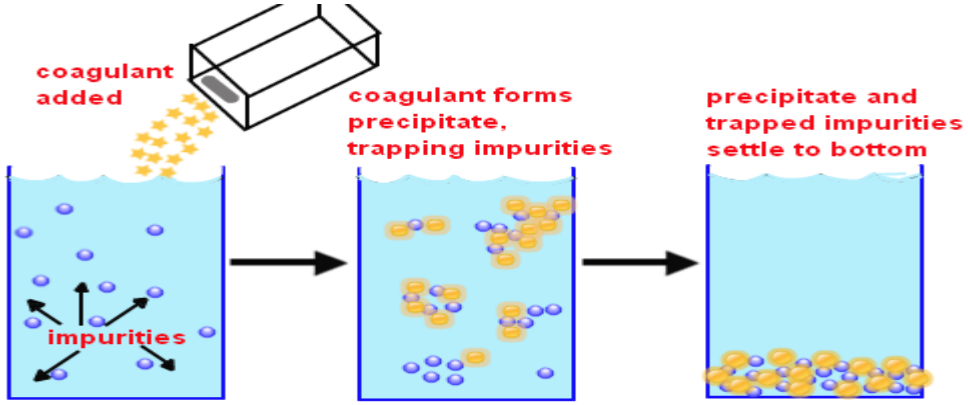

Figure 4: Coagulation-flocculation process (Redah, 2016)

The most widely used chemical coagulants or cationic salts are aluminium(III)(Al^{3+}) and iron(III) salts (Fe^{3+}). Examples are iron sulfate, (Fe_2Cl_3), iron chloride ($Fe_2(SO_4)_3$), aluminium sulfate or as commonly called alum ($Al_2(SO_4)_3.14H_2O$), and polyaluminum chloride $Al_2(OH)_3Cl_3$. The coagulation-flocculation process has good removal efficiencies and short detention time but is limited in its high cost of obtaining chemicals especially for the adjustment of pH and challenges arising from sludge and dewatering handling.

2.3.2 Ion exchange process

This process is a technique of segregation, decontamination and purification of solutions containing ions. This is an irreversible chemical process that has been long used in chemical and engineering fields. It is the exchange of ions (as its name implies) between two electrolytic solutions or between a complex and an electrolytic solution. These ion exchangers include soil humus, zeolites, clay, ion exchange resins, montmorillonite which are mainly either cationic exchanger that exchanges positively charged ions or anionic exchangers for ions that are negatively charged. Softening and deionization are the major methods of ion exchange (Oleiwi, 2014). The softening reduces the hardness of water then the deionization takes place. Alongside adsorption and absorption processes, an ion exchange process is also categorized as a sorption process hence its technology can be used in a column loaded with ion exchange resins (Najm & Trussel, 1999). When the untreated water is passed through the resin column, an exchange takes place between the ions present in the untreated water and that found on the resins. These resins are regenerated by backwashing (washing with excess of the ions) to remove accumulated solids (Kansara et al., 2016). The advantage of this process includes easy regeneration with less depletion of adsorbents, cost-effective, and effectively removes dissolved inorganics. The disadvantages arise from contaminations from non-ionized organic compounds, bacteria and chlorine. A constant build-up of organic matter serves as a growing bed for bacteria.

2.3.3 Advanced Oxidative Process

Advancement in wastewater treatment has given rise to the development of a wide range of operations called advanced oxidative processes (AOPs). These chemical treatment operations devised to eliminate inorganic and organic impurities in

wastewater by reactions with hydroxyl radicals (oxidation). Most AOPs make use of O_2, H_2O_2, or O_3 as strong oxidants to produce the hydroxyl radicals. Among other free radicals, hydroxyl radicals play a central role in AOPs due to its standard potentials that is high as against the standard hydrogen electrode (NHE) in an acidic media (2.8V) and in a basic media (1.55V), high reactivity and non-selectivity (Deng & Zhao, 2015; Wang & Xu, 2012). Generation of the hydroxyl radicals is mostly accelerated by combining H_2O_2, O_3, and TiO2, ultrasound, electron-beam irradiation and UV radiation. Figure 5 illustrates an outline of different developing and approved AOPs, categorized into electrochemical (eAOP), UV-based, ozone-based, physical (pAOP) AOPs, and catalytic (cAOP). The processes are remarked as tested at lab-scale (black), conclusively proven entirely (white), and examined at pilot-and lab-scale (grey)

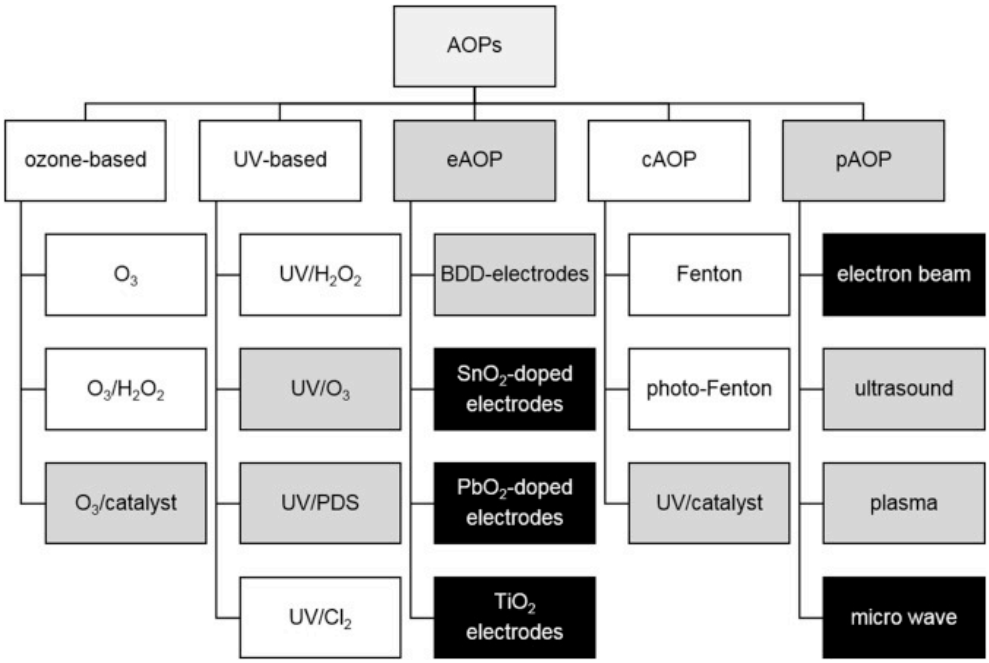

Figure 5: Scope and categories of different AOPs (Miklos et al., 2018)

AOPs generally comprises of two major steps, first are the original formation of oxidative species that are reactive and lastly are the reaction of these reactive species with the destination impurities. The radical formation mechanism is process specific parameters dependent. AOPs have been engaged for the eradication of aromatic compounds, dyes, pharmaceutical compounds, pesticides and even heavy metals. They could be employed as a pretreatment and/or post-treatment stage in the treatment of wastewater to produce biodegradable compounds hence versatile in its applications. However, AOPs are not perfect and so have some setbacks like high capital and cost of operations, complexity of chemical reactions and removal of excess oxidants like H_2O_2 which could have an adverse effect on the subsequent treatment steps.

2.3.4 Biological Methods

Biological methods of treatment anchors specifically on degradation microbially. They are advantageous for treating high organic content wastewater. This treatment method can be categorized into two classes; anaerobic and aerobic processes. The process of organic pollutants degradation found in the wastewater with the use of microbes in the existence of oxygen is termed the aerobic process while that of the anaerobic process is done under insufficient oxygen. The potency of this treatment method is determined by the capability of the solid-fluid disengagement of the biomass and the microbes ability to degrade (Joshiba et al., 2019). The biological treatment system can also be classified into conventional systems such as activated sludge process, packed bed and trickling bed bioreactor systems, and advanced treatment systems such as membrane-based bioreactor, two-phase portioning bioreactor, and cell-immobilized systems (Kanaujiya et al., 2019).

The aerobic digestion can serve as a natural oxidation process as such it is rapid and efficient but requires a lot of energy and problem arises for the disposal of resultant bio-solids or sludge. The anaerobic process is environmentally friendly, requires less energy and produces less biomass and biogas (methane) that could be recycled. Nonetheless, it is less efficient due to its slow process.

2.3.5 Adsorption process

Amongst the above listed, the adsorption process is an effective technique for elimination of a multiplicity of solutes from water removal due to its economic feasibility, i.e. low capital, simple design, and low operational cost (De Gisi et al., 2016; Malik, 2004). Adsorption is a surface anomaly adopted for elimination of a wide range of compounds from wastewater. Adsorption is said to have occurred when the absorbate bind to the highly porous surface of the adsorbents (Rashed, 2013). Generally, adsorption is described as the surface build-up of adsorbate (molecules to be adsorbed from wastewater) on adsorbent (solid on which molecules are retained). The type of the bonding of adsorbate unto the adsorbent is dependent on the features of the type of species concerned, and as result adsorption can occur by physisorption (i.e. weak Van Der Waals forces), electrostatic, or chemisorption (covalent bonding) attractions (Rashed, 2013).

The concept “adsorption” was first suggested by Emil du Bois-Reymond and introduced by Adolph H. Kayser in 1881 to differentiate intermolecular penetration from surface accumulation hence asserting that the essential characteristics of adsorption are the aggregation of substances on a surface (Gupta et al., 2009). Adsorption is of two types namely; physical adsorption (attraction forces are weak van der Waal forces which can be reversible) and chemisorption (force of attraction is due to chemical bonding which is difficult to remove). The simplicity of design,

flexibility (removal of wide variety of target contaminants), allay of operation and impassivity to toxic impurities give adsorption process a great advantage. However, regeneration difficulties and costly disposal of adsorbent pose a problem for this process.

Table 2: Treatment methods and pollutants removed

Treatment Method	Important Feature	Pollutants removed	References
Coagulation and Flocculation	To improve the properties of the floc, removal rate as well as decrease the precipitation time, inorganic coagulant (polyaluminum ferric chloride) and organic flocculant, cationic polyacrylamide were combined	TiO_2 nanoparticles	(You et al., 2019)
Ion Exchange	The use of cationic exchange resin, Amberlite IR-120	Lead	(Alguacil, 2019)
Advanced Oxidative processes (AOPs)	The use of Fenton, Fenton-like, ozone, and peroxone processes with the influence of solid particles, zeolites HY and NH_4ZSM5, on the efficiency of the removal	Azo dyes	(Papic et al., 2006)
Biological process	The use of conventional activated sludge and membrane bioreactor	Antimicrobials and antibiotics	(Tran et al., 2016)
Adsorption process	The use of spent coffee grounds	Heavy metals	(Ayala & Fernandez, 2019)

2.4 Adsorption techniques

Adsorption techniques can be grouped into a batch and continuous fixed-bed techniques on the basis of their modes of operation. The batch technique of adsorption is a discontinuous process carried out under different process criteria like duration, influent concentration, temperature, pH, and dosage for optimization (Noreen et al., 2013). The batch mode operations give an idea into modulating a

column design. The batch method is illustrated as thus, a mass of the adsorbent prepared is combined instantaneously with a desired volume of solution, under agitation for a suitable duration. The emerging solution is then separated by centrifuging, filtering, use of magnets and/or decanting. For the fixed-bed or column adsorption the solution is allowed to permeate through a vertically positioned column as shown in Figure 6 which correlates with the model in the ion exchange columns.

The adsorption capacity for a batch technique is described as the quantity of pollutant per mass of adsorbent at equilibrium. While that for fixed-bed techniques, it is the magnitude of pollutant held back in the bed at exhaustion point per mass of adsorbent (Dichiara et al., 2015). Table 3 explains the features and differences between the discontinuous/ batch and the continuous fixed-bed processes.

Table 3: Features of the adsorption techniques

Adsorption techniques	Batch Process	Continuous Fixed-bed process
Explanation	At a constant volume, the adsorbent and adsorbate are well-mixed in a diluted solution	The adsorbate is continuously flowed through a bed or column of adsorbent at a constant rate
Process Parameters	Temperature, duration, pH, initial concentration, and dosage	Influent adsorbate concentration, pH of adsorbate, adsorbate flowrate, bed height, temperature and adsorbent particle size
Application	This technique can be used to analyze the practicability of the adsorbent-adsorbate system	Can be used for bulk adsorption process and also for industrial purpose, since there is constant contact between the adsorbate and a given quantity of fresh adsorbent
Advantage	This process provides useful data and parameters on the application of specific adsorbents The loaded adsorbent can be gotten from the solution by simple methods as filtration	A simple and efficient process It is important as it provides practical operational information. Also higher contact time and improved mass and heat transfer characteristics.
Disadvantage	Only employed for a small quantity of wastewater that has minimum pollution load; hence it is scarcely found in practical applications	Wearing down (erosion) of adsorbent, feed channelling, and non-uniform flow of adsorbent particles

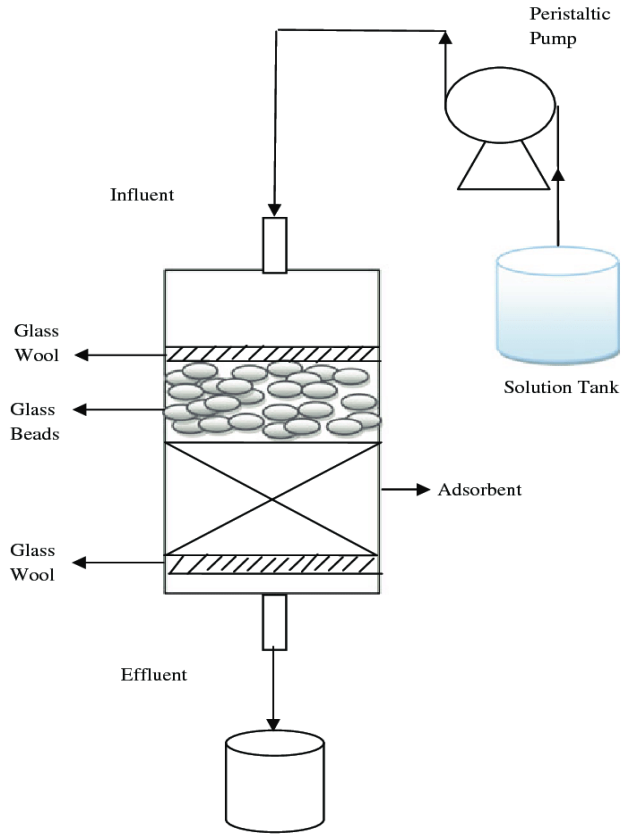

Figure 6: Schematic Diagram of column adsorption (Kapur & Mondal, 2016)

Batch adsorption processes are used to access the removal efficiency of adsorbents and also to obtain the equilibrium isotherms. Figure 7 shows the possible isotherms that can be obtained for a given batch adsorption studies. Breakthrough curves are designed to study the efficiency of column processes. It describes the vital behaviour of the column process (Miralles et al., 2010). Their adsorption mechanism depends on various phenomena, like film diffusion resistance, axial dispersion, adsorption equilibrium with the adsorbent, and diffusion resistance (for both surface and pore diffusion). Adsorption by column method of operation commonly exhibits a characteristic 'S' shape breakthrough curves although with steepness of varying degrees.

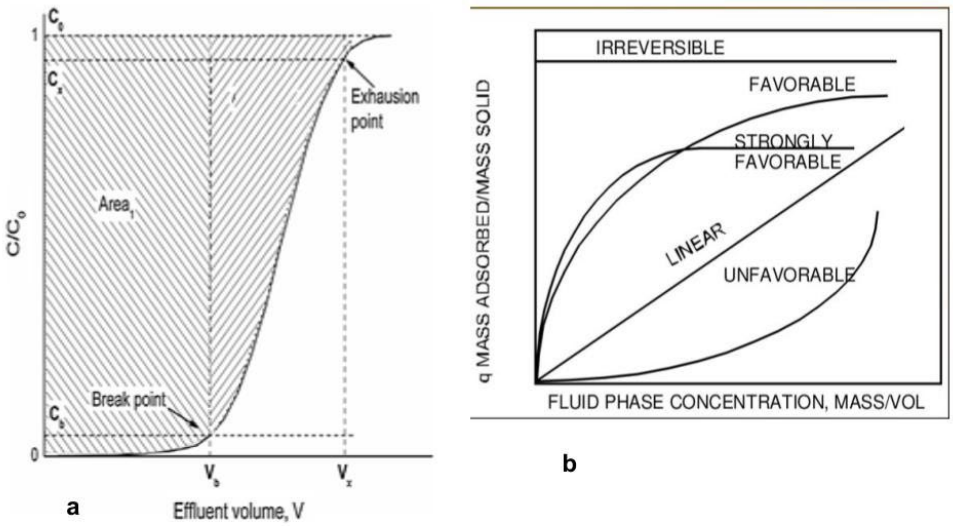

Figure 7: (a) an ideal breakthrough curve, (b) adsorption isotherms (Patel, 2019)

Figure 7 details a model breakthrough curve indicating the scope of the column is absolutely appropriated. The breakthrough point concentration C_b is selected forthwith at a low magnitude. The adsorbent is virtually exhausted when the exhaustion point or effluent concentration C_x is approaching approximately 90% of influent adsorbate concentration C_o. The volume of effluents V_x and V_b correspond to the volume at effluent point concentration and breakthrough point concentration respectively.

2.5 Type of adsorbents

Adsorbents can be generally categorized into three classes namely;

- Natural adsorbents; they include agricultural wastes, plant roots, leaves, etc. The adsorption capacity can be comparatively low
- Synthetic adsorbents; synthesized in the laboratory and although they have high adsorption capacities, the production cost is relatively high
- Semi-synthetic adsorbents; here natural adsorbents undergo physical as well as chemical activation to improve the porosity of the absorbents. They have

high efficiency, the production cost is low, biological or chemical sediment is minimized, and absorbent can be regenerated (Patel, 2019).

Adsorbents can further be categorized on the basis of the nature of the adsorbents: carbon-based adsorbent, oxygen-containing adsorbent, and polymer-based adsorbent. Carbon-based adsorbents like activated carbon and graphite are non-polar and hydrophobic. Oxygen-containing adsorbents like silica gel and zeolites are polar and hydrophilic. While polymer-based adsorbents like polymers and resins could be non-polar and polar depending on the type of functional groups found on the backbone.

2.5.1 Activated Carbon

Adsorbents are distinct in there features like their pore structures, porosity, and nature of their adsorbing surfaces. Amongst all adsorbents, activated carbons stand out most useful by virtue of its comparative removal ability and specific surface area that is high as well as low cost (Pugazhenthiran et al., 2016; Wajima, 2017). Activated carbons are a type of graphite crystallites with amorphous or random structures that are highly porous. Activated carbons (ACs) can be in granular, powdered, fibre or fabric (Tripathi et al., 2018), and spherical forms. 95% of its mass weight is carbon which is its main constituent while the others contain heteroatoms such as oxygen, hydrogen, sulfur and nitrogen. ACs can be obtained from carbonaceous materials like wood products, lignite coals, petroleum coke, olive stones, palm fronds, coconut shell and fibres (Ahmad et al., 2010; Yakout & El-Deen, 2016). Activated carbon is prepared from its source material using two common activation processes. First is physical activation where the source material is subjected to pyrolysis and then activation or in some cases both. In carbonization, the source material is thermally decomposed at temperatures ranging from 600-900^{o}C in a chemically inactive atmosphere producing char. For the process of

activation the source material is first exposed to oxygen, steam, or carbon dioxide in 600–1200°C temperature range, resulting in the elimination of the more disorderly carbon atoms forming a well-enhanced structure possessing a surface area as high as 2500 m^2/g and good porosity. The second is activation chemically which includes impregnation of source materials with NaOH, H_3PO_4, HNO_3, or KOH chemicals, and afterwards heating at 450 to 900°C temperature range of under the flow of nitrogen gas. The activation done chemically is often adopted over that done physically due to lesser time of activation and lower temperature ranges (Gupta et al., 2009).

Activated carbons possess a range of heterogeneous pore diameters. Present in the highly porous internal structures of activated carbons are meso (2–50 nm), macro (>50 nm), and micro (<2 nm) pores. It's high surface area which is imparted by its high porosity structure results in an enormous amount of reactive sites needed to interact with the adsorbate species. The type of precursor material, method of activation and other modifications determine the type of internal pore composition of the activated carbon. The conventional composition of elements in activated carbon is approximately carbon (80%), and the remaining 20% consisting of other elements in very small compositions (Sweetman et al., 2017).

2.6 Low-cost adsorbents

The quest for adsorbents with low cost and ability to bind to the impurities found in wastewater has heightened in recent years as the commercially available activated carbons are very expensive even though its design and operation can be easily handled. Many research workers have made attempts to control pollution to obtain cheaper alternative adsorbents. They generally target replacing activated carbons with alternative products coming from industrial and agricultural activities (i.e., rice

hulls, petroleum wastes, scrap tyres). These by-products are voluminous and can be toxic in nature hence, present a variety of problems of disposal. The possibility of employing these by-products alternative source adsorbents will yield a two-fold advantage to removal of contaminants from the environment. Firstly, is the reduction in the voluminous by-products and secondly is the reduction in the pollution of wastewaters at moderate cost when they are modified (De Gisi et al., 2016). These alternative adsorbents as explained in Table 4 could include industrial wastes, household wastes, soil and ore materials, sea materials, natural materials, sludge and agricultural wastes (Crini, 2005). This study analyzed the use of saccharide-based materials which are also low-cost as precursors for adsorbents. Particularly banana peels and discarded chewing gum were used here.

Table 4: Examples of low-cost alternative adsorbents and pollutants removed

Sources	Examples	Pollutants Removed	References
Industrial Wastes	Papermill sludge	sulfamethoxazole, carbamazepine, and paroxetine	(Jaria et al., 2019)
	Fly ash (coal combustion by-product)	Heavy metals (Cu, Ni, Fe)	(Hegazi, 2013)
	Scrap tyres	Rhodamine B	(Li et al., 2010)
Agricultural and household wastes	Rice husk	Heavy metals (Cu, Ni, Fe)	(Hegazi, 2013)
		malachite green	(Ramaraju et al., 2014)
	Lemon peel	Copper ions	(Meseldzija et al., 2019)
	Peanut hull	Reactive dye	(Tanyildizi, 2011)
	Coir pith	Congo red	(Namasivayam & Kavitha, 2002)
	Corn hobs	Tyrosine and Phenylalanine	(Alves et al., 2013)
Sea materials	Seaweed	Fluoxetine and Venlafaxine	(Silva et al., 2019)
	Peat moss	Sonocatalytic reduction of rhodamine B	(Kim et al., 2018)
Soil and ore materials	Clay	Lead and cadmium ions	(Meneguin et al., 2017)
	Zeolite	Benzothiophene	(Sun et al., 2015)
Sludge from wastewater	Sewage sludge	sulfonated methyl phenol resin	(Liu et al., 2015)
Novel low-cost adsorbents	Cyprus spent coffee	Tetracycline and phenol	(Oladipo et al., 2016)

2.7 Banana Peel as Adsorbent

Banana plants are of the family *Musaceae* with the *Australimusa* and *Eumusa* series the suitable species for consumption. The readily available and edible ones belongs to the *Musa accuminata* species of banana (Mohapatra et al., 2010). This highly nutritious fruit is majorly produced in the tropical regions like Ecuador, China, India, Brazil, and Philippines. Wastes from banana as a whole are interestingly important

amidst other agricultural wastes, as the number of banana produced and eaten on a daily basis keeps increasing. The peels alone make up about 40% of the banana as a whole (Ahmad & Danish, 2018; Yu et al., 2018). However, these wastes from banana peel can cause offensive odour, dangerous accidents and also produce greenhouse gases if not managed properly (Shah et al., 2005). Its ultra-high carbohydrate content makes it ideal as precursor for alternative low-cost and value-added adsorbents. Banana peel wastes are said to possess an array of functional groups (i.e. carboxyl, amide, and hydroxyl groups) that occur on their surfaces, and seemingly perform an essential purpose in the process of adsorption (Liu et al., 2012). Experimentally, banana peels have been confirmed to be a good derivative of pectin (10–21%), cellulose (7.6–9.6%), lignin (6–12%), galacturonic acid hemicelluloses (6.4–9.4%) (Ahmad & Danish, 2018). These banana peel waste has also been used as landfills.

Banana peel wastes have been largely explored for the adsorption of a large range of water contaminants. Bibaj et al., (2019) produced both hydrothermal and pyrolyzed activated carbon using banana peel wastes as a precursor for the removal of nickel. The samples were activated with H_3PO_4 at different temperature ranges. The adsorption efficiency of the pyrolyzed product at pH 6 was slightly greater than that of the hydrothermal product. The sorption performance of banana peels were investigated for an effective oil spill cleanup (El-Din et al., 2018). Castro et al., (2011) reported on the adsorption of Cu^{2+} and Pb^{2+} ions using wastes from banana peels which exhibits transmittance peaks of carboxylic (1730 cm^{-1}) and amine (889 $cm^{-}1$) groups. Their optimum adsorptions at pH > 3 within 10 min were 41.44 (Pb^{2+}) and 20.97 mg/g (Cu^{2+}). Banana peel wastes have been severally employed as an effective low-cost alternative adsorbent (Ali & Saeed, 2016; Castro et al., 2011;

Munagapati et al., 2018). The problem arises from difficulties in their separation from resultant solution due to their low specific gravity and inclination to aggregate. This limitation has been greatly resolved by magnetic separation which utilizes an extrinsic magnetic field (Gazi et al., 2018; Lasheen et al., 2016; Oladipo & Gazi, 2015a; Oladipo & Ifebajo, 2018; Oladipo et al., 2019).

2.8 Discarded chewing gum

Chewing gum is made up of gum base which is composed of polymers (like elastomers, which are responsible for the stretchy and sticky nature), resins (the hydrophobic portion of the gum base responsible for its chewiness), and plasticizers (which improve the flexibility and reduce brittleness, contributing to the plastic and elastic nature of the gum). The discarded chewing gum is a notorious environmental waste which is difficult to deal with. In fact, the discarded chewing gum is a major and increasingly growing social and environmental issue due to its high stickiness and longer years to biodegrade. Chewing gum is not compostable; it rather piles up even when digested it is expelled from the digestive tract undigested. Discarded chewing gum is the next biggest litter worldwide after cigarette butts. It makes our environment grubby, injure our wildlife (birds could mistake it for bread crumbs and it clogs their digestive system when eaten) and also uses up a massive portion of our public budgets as the money required to clean up the gums off the street much higher than that required for its production. It poses a challenging problem such that countries like Singapore have banned the use of chewing gum except with a prescription from a doctor or dentist.

Discarded chewing gum has been converted to other useful products like plastic due to the non-decomposable polyisobutylene in chewing gum but invariably plastics

which do not degrade are produced hence a chain of disposal problems (Dragani, 2019; Oladipo et al., 2019). Production of biodegradable chewing gum has also been a way of easy disposal but this can be costly. In this thesis, the discarded chewing gum was utilized for producing low-cost alternative adsorbent. Until now, no study has reported this application for discarded chewing gum.

Chapter 3

EXPERIMENTAL

3.1 Materials and Reagents

Analytical grade chemical reagents are utilized without further purification. The discarded chewing gums were collected from the surroundings of Eastern Mediterranean University, Famagusta North Cyprus while the banana peel wastes were obtained from the locality of Famagusta, North Cyprus. Silver nitrate ($AgNO_3$, >98%), hydrogen peroxide (H_2O_2, 30%), potassium bromide (KBr, 99%), sodium hydroxide (NaOH, 99.9%), hydrogen chloride (HCl, 37%), $FeSO_4$ (99.9%), ammonia solution (25%) (Aqueous), ferric chloride (99.5%), mercury chloride ($HgCl_2$), zinc (II) nitrate hexahydrate ($Zn(NO_3)_2.6H_2O$), Hydrochloric acid (37%) sodium hydroxide and copper (II) sulfate pentahydrate ($CuSO_4.5H_2O$) were supplied by Sigma-Aldrich (Germany). 2,4,5-Trichlorophenol (2,4,5-TCP, 98.9%) was purchased from Carlo Erba reagents (Spain). The water was used in all procedures were double-deionised and the needed concentrations of solutions were processed by precisely mixing weighed samples of materials in the double-distilled water. The test solutions were produced using deionized water from an already prepared stock solution of 500 mg/L, and solution pH were varied by either adding NaOH or HCl (both 0.01 N).

3.2 Preparation of Adsorbates

Stock solutions (500 mgL^{-1}) of heavy metals (Cu, Hg, and Zn) and 2,4,5-TCP were produced by mixing the pre-calculated amount of the metallic salts and pure 2,4,5-TCP compounds respectively in the double-deionized water. The diluted solutions

used were freshly prepared from the initial bulk solutions via serial dilutions until desired concentration (2-200 mgL^{-1}) obtained. For each of the adsorbate, a calibration curve was plotted, and the necessary working data were extracted.

3.3 Preparation of Adsorbents

The adsorbents used are calcined biomass and calcined magnetic biochar based on banana peels and discarded chewing gum-derived pyrochar/AgBr

3.3.1 Preparation of calcined biochar (CB)

The wastes of banana peels were initially well-cleaned with double-distilled water to clean off impurities on it and then, cut into uniform sizes before it is put in a conventional oven for 24 h at 90 ºC to dry properly. The properly dried samples were crushed and sift through a typical 60 mesh sized sieve in the laboratory to obtain a powder of uniform size which was further calcined in a muffle oven for a duration of 2 h at 500 °C, and afterwards cooled for later use. The resulting calcined biochar which is non-magnetic was denoted as CB.

3.3.2 Preparation of magnetic calcined biochar (MCB)

The MCB was processed using a typical co-precipitation method obtained from other works (Oladipo & Gazi, 2015b; Oladipo & Ifebajo, 2018). Ordinarily, CB (10 g) was combined with the solution (200 mL) comprising of $FeSO_4 \cdot 7H_2O$ of 4 g and $FeCl_3 \cdot 6H_2O$ of 6 g, and homogenized by stirring continuously at 50 °C for 30 min. At the lapse of the 30 min, 2 M NaOH was introduced into the mixture dropwise as the stirring continued till 60 min at same temperature. Afterwards the magnetic biomass was easily gotten by using an external magnetic field to separate it from the resulting solution and then severally washed to obtain a filtrate with pH of ~7.0 with ethanol and distilled water. The leftover after filtration was then dried for 36 h at 50 °C and further carbonized again for 1 h at 800 °C to get the MCB.

3.3.3 Preparation of pyrochar/AgBr based on discarded chewing gum

The pyrochar was produced from discarded chewing gum (of no specific origin) from a reported pyrolysis process (Monlau et al., 2015). Briefly, 5 g of pre-washed and dried discarded chewing gum was fed into a crucible and heated under an inert condition. The pyrolysis at 500 °C was done for 2 h. 3 g of the pyrochar obtained was mixed with 30 mL of $AgNO_3$ (0.25 M) and stirred continuously at 30ºC for 30 min. Afterwards, 10 mL of KBr (0.125 M) was introduced dropwise. The solution was then irradiated in a microwave for less than 5 min and then filtered, severally flushed with ethanol-acetone mixture and dried overnight at 60 °C. The outcome, pyrochar/AgBr was pulverized, sieved to a uniform size and stored well for later use.

3.4 Characterization of as-prepared adsorbents

Characterization of the biochar were performed using a JSM-6390 SEM (JEOL, Japan) furnished with an EDX (energy dispersive spectroscopy) functionality. Functional groups located on the biochar were identified with an FTIR- 8700 spectrophotometer (Perkin-Elmer, Japan) possessing the range of 4000–400 cm−1. The surface properties and pore distribution were evaluated on an Autosorb analyzer (QuantaChrome, USA) at a temperature of −196 ºC. The crystallinity at 50 kV monochromatic radiation was gotten using an XRD (Bruker D8) with a Cu Kα (λ=1.54187 Å). The ASTM standard procedure was used to determine Boehm analysis (Oladipo & Gazi, 2015a, 2015b; Zaghouane-Boudiaf & Boutahala, 2011), pH points zero charge (pH_{pzc}), and physicochemical features.

3.5 Sorption Experiments

3.5.1 Batch experiments for Cu^{2+}, Zn^{2+} and Hg^{2+} removal with CB and MCB

The metallic bulk solution (1000 mg/L) was first processed with known amounts of $CuSO_4 \cdot 5H_2O$, $HgCl_2$, and $Zn(NO_3)2 \cdot 6H_2O$ for Cu^{2+}, Hg^{2+} and Zn^{2+} respectively in a

distilled water. The linear calibration curves were acquired with R^2 ≥0.998 from prepared diluted solutions.

For the batch processes, the already weighed adsorbents were put in Erlenmeyer flasks (250 mL) containing the metal ions solution of pre-determined concentrations and agitated at 200 rpm. The loaded CB was filtered out while the loaded MCB removed with an external magnetic field and their filtrates were evaluated for the magnitude of metal ions left after adsorption. The influence of dosage (0.2-1.0 g), influent concentration (50–200 mg/L), and duration (10-360 min) were examined at room temperature. Experiments were run in triplicates and the average value noted at an average standard deviation of 1.1%. The removal efficiency, R (%) of the biochars and removal capacity, q_e (mg/g) were evaluated from other studies (Oladipo & Gazi, 2015a, 2015b)

Removal capacity $q_e = \frac{(C_i - C_e)V}{m}$ (1)

Removal efficiency $R = \left[\frac{C_i - C_e}{C_i}\right] 100$ (2)

Where C_i and C_e are the initial and equilibrium concentrations, V is the volume of the solution and m is the mass of the adsorbent.

3.5.2 Fixed-bed column adsorption studies of 2,4,5-TCP with pyrochar/AgBr

A polyvinyl carbonate syringe tube of 10 cm bed height and 1 cm internal diameter was used for the fixed-bed adsorption. The bed was loaded with a pre-determined amount of pyrochar/AgBr between two supporting glass wools to avoid loss of adsorbent. The pyrochar/AgBr loaded-columns were first elated with distilled water for 30 min to stabilize the beds and eliminate air bubbles and. The effect of significant parameters such as flow rate (1–10 mL/min), influent 2,4,5-TCP concentration (20–100 mg/L), depth of bed (1–3 cm) and H_2O_2 concentration (0.1–5

mM) on the breakthrough curves and quantity of 2,4,5-TCP adsorbed were evaluated.

The column processes were performed at 25 ^{o} C and the control valve was used to regulate the flow rate. The solution pH for all the fixed-bed experiments were fixed at 6. The effluent was collected periodically and the remaining 2,4,5-TCP concentration was determined at λ_{max} = 290 nm.

3.6 Fixed-bed data analysis and breakthrough performance modelling

The measurements were done in triplicates with the average results stated. The equations used to evaluate the fixed- bed adsorption information (Oladipo et al., 2016) are as follows.

Total quantity of 2,4,5 - TCP sent to column $(M_{tot}) = \frac{C_i V_{eff}}{1000}$ (3)

Total 2,4,5 - TCP adsorbed in column $(M_{ads}) = F \int_{t=0}^{t=total} C_{ads}\, dt$ (4)

Total 2,4,5 - TCP removal efficiency (%) $= \frac{M_{ads}}{M_{tot}} \times 100$ (5)

Overall adsorption zone $(\Delta t) = t_e - t_b$ (6)

mass transfer zone length $(Z_m) = Z\left[1 - \frac{t_b}{t_e}\right]$ (7)

Here, F is the rate flow (mL/min) of 2,4,5-TCP, Z is height of bed (cm), C_{ads} is the 2,4,5-TCP concentration adsorbed, C_i and C_e is influent and effluent concentration respectively and t_b, t_e is breakthrough time (C_e/C_i= 5.1%) and exhaustion time (C_e/C_i= 94.9%) (min), respectively. To elucidate the mechanism of 2,4,5-TCP removal by pyrochar/AgBr and predict the breakthrough performance, the fixed-bed adsorption data were examined using empirical models e.g. Bed Depth Service Time (BDST), Thomas, Clark, Adams-Bohart, Yoon-Nelson, and Dose-response (Abdolali

et al., 2017; Oladipo et al., 2016; Rouf & Nagapadma, 2015). It's worthy to mention that in the preliminary studies, pyrochar/AgBr exhibited relatively higher performance and lower pressure drop in the column operation compared with pyrochar alone. Hence, subsequent research was conducted with pyrochar/AgBr.

3.7 Adsorption isotherms and Kinetics

Adsorption isotherms illustrate the interactions that ensue amidst the adsorbent and adsorbate species at equilibrium conditions (Inyang et al., 2016). The generally applied isotherms in this study are Freundlich, Redlich─Peterson (R-P), Langmuir, and Temkin as listed in **Table 5**. Where the adsorbate solution is in a multicomponent system, the interaction of adsorbate molecules may affect the sorption capacity of the adsorbents in an interactive manner (Yan et al., 2014).

Table 5: Features of Adsorption isotherm models

Isotherm Models	Equation	Description	Features
Langmuir	$q_e = \frac{q_m b C_e}{1 + bC_e}$	C_e is equilibrium concentration of pollutants (mg/L), q_e is the equilibrium adsorption capacity (mg/g), b is Langmuir constant (L/mg) and q_m maximum adsorption capacity (mg/g).	Assumes monolayer adsorption, where sorption occurs at the large similar active sites and no associations between molecules adsorbed
Freundlich	$q_e = K_F {C_e}^{1/n}$	n is empirical parameter for adsorption intensity and K_F is the Freundlich constant (mg/g)(mg/L)$^{(-1/n)}$.	This model is usually utilized for non-ideal sorption or multilayer sorption
Redlich-Peterson	$q_e = \frac{K_{rp} C_e}{1 + \alpha_{rp} {C_e}^{\beta}}$	K_{rp}, and α are r-p equilibrium constant, β is exponent constant value from (0–1). When(β = 1, R-P equation → Langmuir equation)	This is a three-parameter model that limits errors for Freundlich and Langmuir models
Temkin	$q_e = \frac{RT}{K_T} \ln[A_T C_e]$	A_T and K_T are equilibrium Temkin binding constant, R is gas constant (J/mol.K), T is temperature (K)	This model is only valid for ion concentrations of intermediate range. It accounts for the indirect interactions effects.

The adsorption kinetics determines the rate of the adsorption technique which is dependent on various criteria as it relates to the physiochemical features. It is an essential feature that provides relevant information regarding the routes of reaction. The adsorption kinetics allows for the monitoring of the time of residence at solid-solution intersection by giving indications about the uptake rate of adsorbents (Awad et al., 2019). Table 6 describes various adsorption kinetic models.

Table 6: Adsorption Kinetics models

Kinetic models	Equations	Description
Pseudo First Order	$q_t = q_e(1 - e^{k_1 t})$	The simplest and easiest of all models that describes the rate of adsorption for liquid phase systems
Pseudo second order	$q_t = \frac{k_2 q_e^2 t}{1 + k_2 q_e t}$	This model is used for adsorption processes that includes chemical bonding between the functional species of the adsorbent
Elovich	$q_t = \frac{1}{\beta}\ln(\alpha\beta t + 1)$	Can be used for the modeling of adsorption processes of heterogeneous surfaced adsorbents
Intraparticle Diffusion	$q_t = K_1 t^{1/2} + W$	This determines the rate limiting step

where qe (mmol kg^{-1}) and qt (mmol kg^{-1}) are the amounts of pollutants adsorbed at equilibrium and at time (t) respectively; k_1 (h^{-1}) and k_2 (kg $mmol^{-1}$ h^{-1}) are the first- and second-order constants, respectively; α (mmol kg^{-1} h^{-1}) and β (kg mmol−1) are the initial pollutant sorption and desorption rate constant at time t, respectively; K_1 is the intraparticle diffusion rate constant (mmol $kg^{-1}h^{-0.5}$); and W (mmol/kg) is a thickness of boundary layer constant.

3.8 Desorption and reusability Experiments

Prior to the reuse test, the 2,4,5-TCP– loaded pyrochar/AgBr was eluted by passing 0.1 M HCl or NaOH (0.1M) solution through the drenched bed for 20 min (25 mL/min) followed by 20 mL distilled water after each elution cycle. The eluted pyrochar/AgBr was regenerated at 80 °C and subjected to successive reuse experiments. This was also done for the heavy metal loaded biochar.

Chapter 4

RESULTS AND DISCUSSIONS

4.1 Characterization

4.1.1 Physio-chemical characterization of pyrochar/AgBr

Pyrochar/AgBr exhibited type I and IV isotherms with an obvious N_2 uptake at comparatively low pressure (P/P_o <0.1) and large N_2 uptake at P/P_o > 0.65 (Figure 8a), suggesting the existence of both micro- (< 2 nm) and meso-pores (2–50 nm) (Serafin et al., 2017; Oladipo et al., 2018b). Also, note that the isotherms do not deflate at a P/P_o ~0.2, confirming the presence of H1 hysteresis loop (Wang et al., 2018). The pyrochar/AgBr possess a high S_{BET} of 249.5 m^2/g (microporous fraction ~ 79.8 m^2/g) and a total pore volume of 0.998 cm^3/g (microporous fraction ~0.31 cm^3/g). It is believed that the pyrochar/AgBr mesopores act as the entry point and transportation pathway for the 2,4,5- TCP, while the micropores serve as the reactive sites for adsorption.

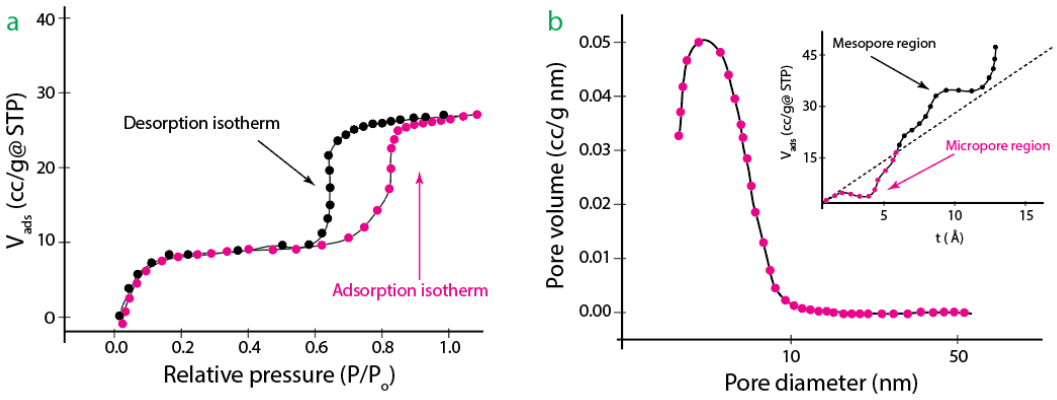

Figure 8: (a) The pyrochar/AgBr N_2 Adsorption–desorption isotherms (b) pore size distribution

FTIR spectra of pyrochar, pyrochar/AgBr before and after adsorption were obtained (Figure 9). The main peaks between 3700–3500 cm^{-1} in the two sample spectra indicates the existence of –OH and C-H stretching vibration bond (Ifebajo, Oladipo, & Gazi, 2019). The small peaks at 1642–1738 cm^{-1} indicate the existence of C=O, C-O_2 and C=C groups (Monlau et al., 2015). Note that the 1218 cm^{-1} peak in the fingerprint region is indicative of the symmetric C-O stretching. The peaks found in the 880-670 cm^{-1} region shows the formation of aromatic C-H bending due to pyrolysis treatment (Monlau et al., 2015). The peak located at 1340 cm^{-1} of the pyrochar/AgBr spectrum is characteristic –Ag-plane (Oladipo et al., 2018). After adsorption, no significant changes were observed except an obvious decrease in the Ag peak, suggesting possible complex formation with the unionized 2,4,5-TCP. McEvoy & Zhang, (2016) reported similar observation, where the Ag in the AgBr-loaded activated carbon formed complexes with the unionized phenol.

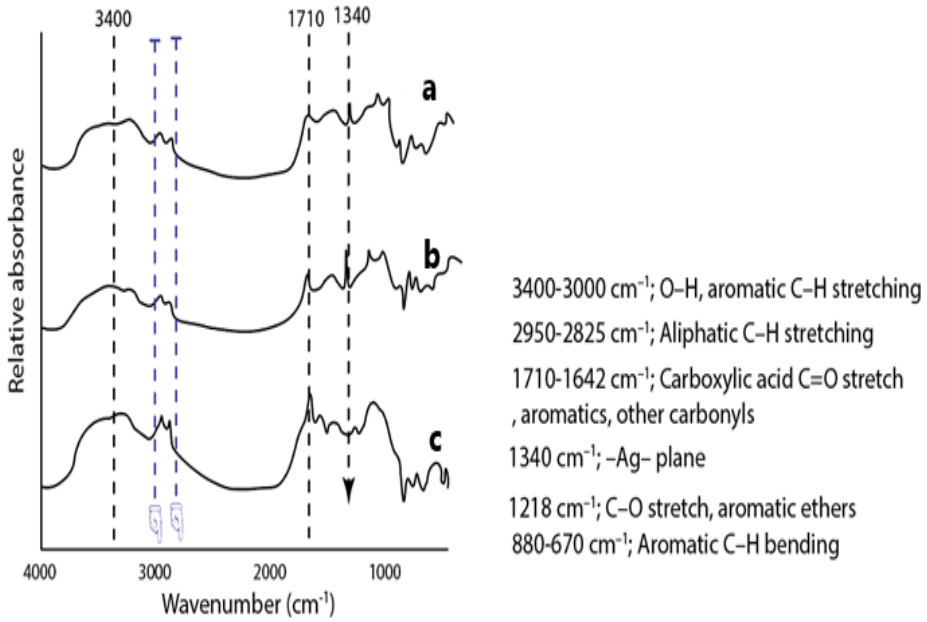

Figure 9: FTIR spectra of (a) Pyrochar/AgBr after adsorption (b) Pyrochar/AgBr before adsorption (c) pyrochar

The surface elemental analysis of pyrochar/AgBr indicates that it contained 83.6% of C-C, 9.75% of C-O, 1.35% of C=O and its polarity index ((O + N)/C) is 0.45. This observation is consistent with the EDX analysis as seen in Figure 10a. The EDX pyrochar spectrum (inset) clearly indicates the presence of oxygen (33.6 wt.%), carbon (60.1 wt.%), nitrogen (5.1 wt.%) and some traces of potassium (1.2 wt.%). The presence of Ag and Br in the EDX spectrum of the pyrochar/AgBr confirmed the successful loading of the AgBr on the pyrochar. The AgBr nanoparticles improved the adsorptive and catalytic detoxification potential of the modified pyrochar. Similarly, McEvoy and Zhang (2016) reported that AgBr loaded onto activated carbon, enhanced the adsorptive and catalytic detoxification of phenol and methyl orange Notably, the concentration of the carbon decreased slightly and the Pt noticed in the spectra originated from the platinum coating during the analysis. From Figure 10b, the scanning electron microscope (SEM) image of pyrochar/AgBr indicates a cranky and lamellar morphology. The enlarged section of the SEM image shows that the pyrochar/AgBr obviously possessed varying porous structures which is consistent with the Brunauer–Emmett–Teller analysis.

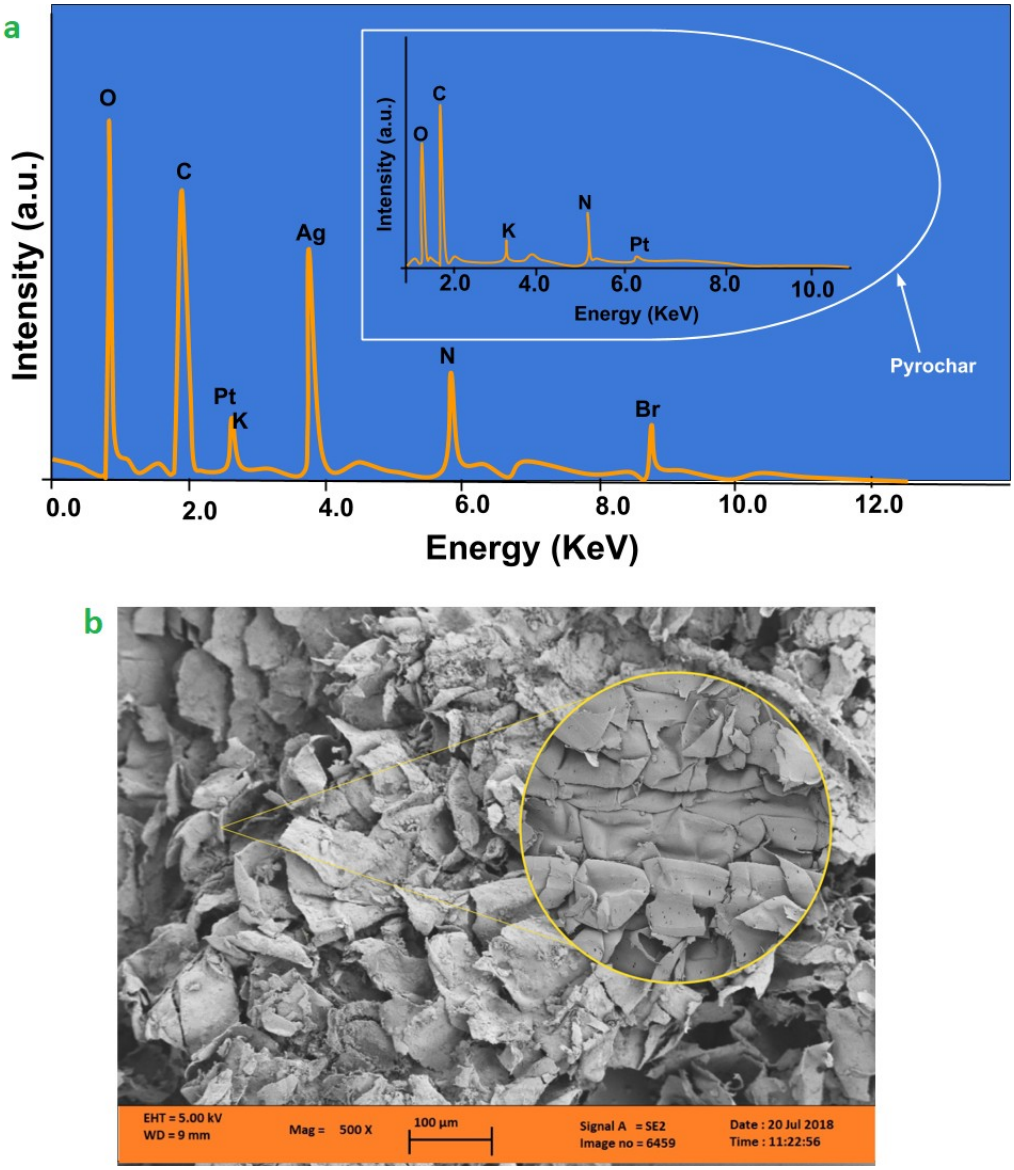

Figure 10: (a) EDX of pyrochar/AgBr and pyrochar (inset) (b) SEM image of pyrochar/AgBr

4.1.2 Characteristics of MCB and CB

CB and MCB have IR bands that are identical as shown in Figure 11a. The figure (a, d) represents CB while (b, c) represents MCB IR bands before and after their adsorptions, respectively. For both CB and MCB, the vibration stretch of free –OH groups were seen in the peak region of 3307-3048 cm^{-1}. The synthesis of Fe_2O_3/Fe_3O_4 on the CB to produce MCB attribute the H–bonded –OH stretching vibrations in possible peaks region of 3300-3400 cm^{-1} (Mohan et al., 2014). Bands in

the 1639–1579 cm^{-1} signifies the C=O vibrational stretch hence the existence of acidic oxygen-containing surface functional groups (–COOH) essential for the metal species adsorption (Pap et al., 2018). The $–CH_2$ groups in a carboxylic acid are attributed to bands at 2325 and 2164 cm^{-1} respectively (Zhou et al., 2017). The detection of the stretching vibration of the phenolic –OH resulted from bands at 1457–1415 cm^{-1} (Wang et al., 2015), which was not noticed in MCB because it weakened till it disappeared at increasing temperature above 600 °C. Similar to Jiang et al., (2015), the peaks at 1117–1287 cm^{-1} indicates C–O bond stretching indicating the presence of carboxylate anion. The presence of π-electron was indicated at bands region between 880 and 753 cm^{-1} which are given to aromatic CH and evident for CB but in MCB it depleted (Faheem et al., 2016; Sizmur et al., 2017; Wang et al., 2015).

The IR bands located at 434 and 525 cm^{-1} which is distinct for MCB spectrum indicates the stretching Fe-O group vibration of Fe_3O_4 (Oladipo & Gazi, 2015a; Oladipo & Ifebajo, 2018). As seen in Table 7, MCB possesses limited quantity of the surface acidic functional groups due to its calcination at 800 °C resulting in stronger and broader peaks of carboxylic and hydroxyl groups noticed for CB than for MCB. Following the adsorption of metal ions on the adsorbents, the strengths of functional groups reduced and the C=O band weakened, indicating surface complexation.

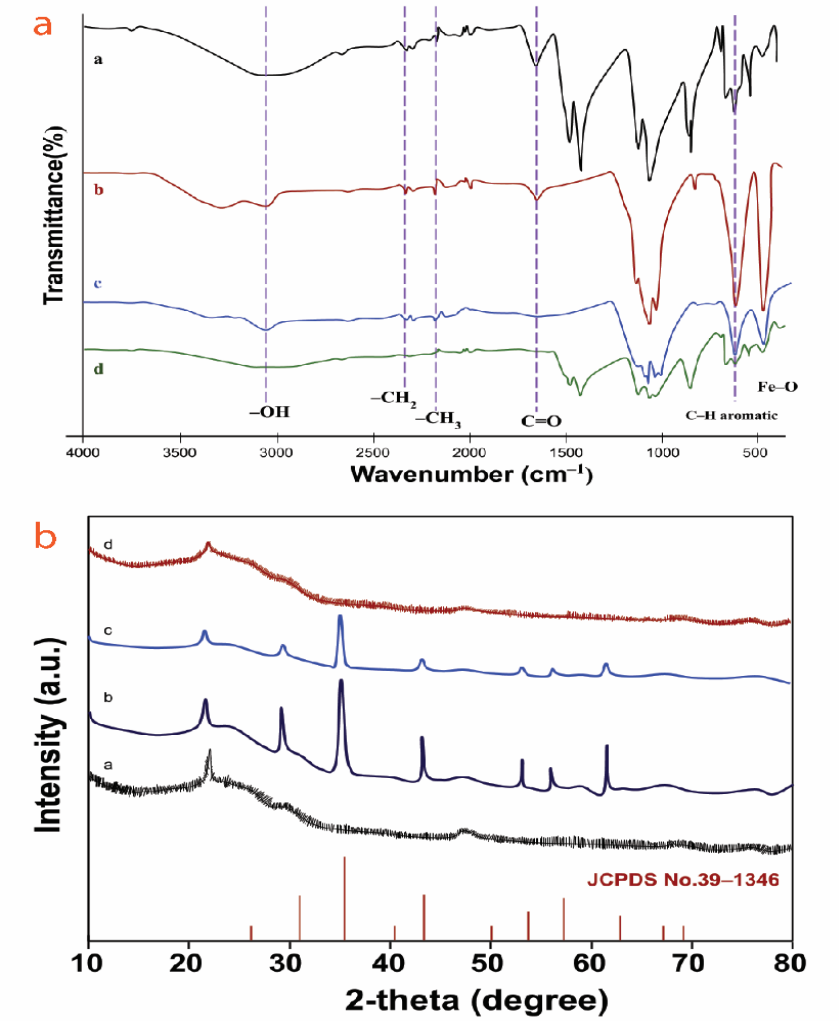

Figure 11: (a) FTIR bands of adsorbents where (a, d) is CB and (b, c) is MCB before and after adsorption, respectively. (b) XRD patterns of samples (a: CB; b: MCB before adsorption) and (c: CB; and d: MCB after adsorption)

The XRD patterns shown in Figure 11b displays an exceptional crystallinity for MCB as relates with CB. From the figure, patterns a & b represents CB and MCB before adsorption while c and d represent CB and MCB after adsorption respectively. Both adsorbents exhibited a corresponding plane of the biochar graphic crystal plane to a broad diffraction peak at ~ 24° (Rong et al. 2019). Indexed to (440), (511), (422), (400), (311), and (220) planes of cubic magnetite (Fe_3O_4) (JCPDS no. 39–1346) are evident reflections observed at 2θ = 31.9, 35.9, 43.9, 53.9, 57.7, and 63.2° for MCB respectively (Li et al., 2019; Rong et al., 2019). Note that after the adsorption, the XRD peaks intensities weakened.

Table 7: Textural and physicochemical properties of the MCB and CB

Parameter	Unit	CB	MCB
Elemental analysis			
C	(%)	70.11	73.09
O	(%)	15.11	11.01
N	(%)	0.89	0.52
H	(%)	5.21	3.02
K	(%)	6.91	0.29
Fe_{bulk}	(%)	1.22	5.02
Fe_{suf}	(%)	0.55	7.05
Surface acidic functional groups			
Carboxylic	mmol/g	6.14	5.69
Phenolic	mmol/g	3.78	2.28
Moisture content	(%)	2.81	1.09
Ash content	(%)	3.43	2.11
pH_{pzc}		5.05	4.53
pH_{sef}		7.06	9.10
S_{BET}	m^2/g	95.89	323.2
Mesopore volume	cm^3/g	0.11	0.21
Micropore volume	cm^3/g	0.08	0.13
Total pore volume	cm^3/g	0.19	0.34
Average pore diameter	Nm	11.88	8.83
Specific saturation magnetization	(emu/g)	0.0	39.55

As shown in Figure 12a, the concurrence of mesopores and micropores is indicated by the isotherms of type I and IV exhibited in conformation to the classification of IUPAC (Serafin et al., 2017). The adsorbents showed the H4 hysteresis loop, indicating mesopores that are narrow slit-shaped and exhibited slopes that are higher (0.8 to 1.0) in relative pressure (Zhong et al., 2016; Oladipo et al., 2019). The total volume of pore (0.34 cm^3 /g) and S_{BET} (323.2 m^2 /g) of MCB are evidently higher than that of CB (95.89 m^2 /g and 0.19 cm^3 /g), contributing positively to the sorption efficiency of MCB.

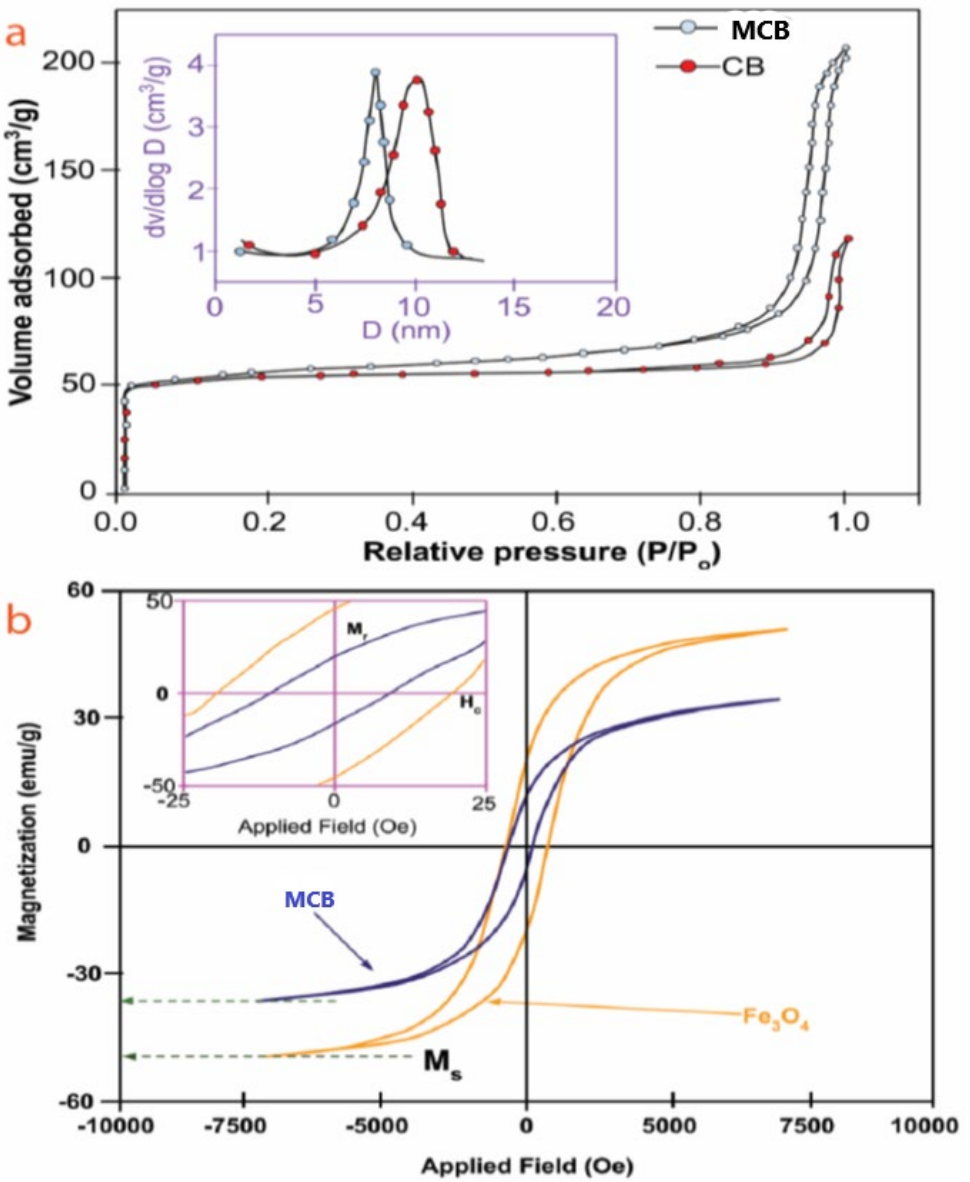

Figure 12: (a) CB and MCB N_2 adsorption–desorption isotherms and pore size distributions (inset). (b) Magnetic hysteresis loops for Fe_3O_4 and MCB, the coercivity (Hc) and remanence (Mr) are inset

The magnetic hysteresis loop for MCB as shown in Figure 12b gives the coercivity (10.63 Oe), specific saturation magnetization (39.55 emu/g), and remanence (26.52 emu/g), which proves MCB can be separated easily utilizing of an external magnetic field. The presence of the calcined banana peel in MCB lowered its magnetic features as compared to Fe_3O_4 (coercivity, 21.22 Oe; specific saturation magnetization 49.51 emu/g; and remanence, 39.55 emu/g). The adsorbents have

similar morphologies (Figure 13a). They both possess irregular cranky lamellar structure which probably emanates from the carbonization and aromatization of the molecules of carbohydrates in the banana wastes (Rong et al., 2019). The mapping of the EDX (Figure 13b) of both adsorbents indicates the existence of C, Mg, O, N, Fe, Ca, and Na peaks with the Fe peaks high in the MCB from Fe_3O_4 presence.

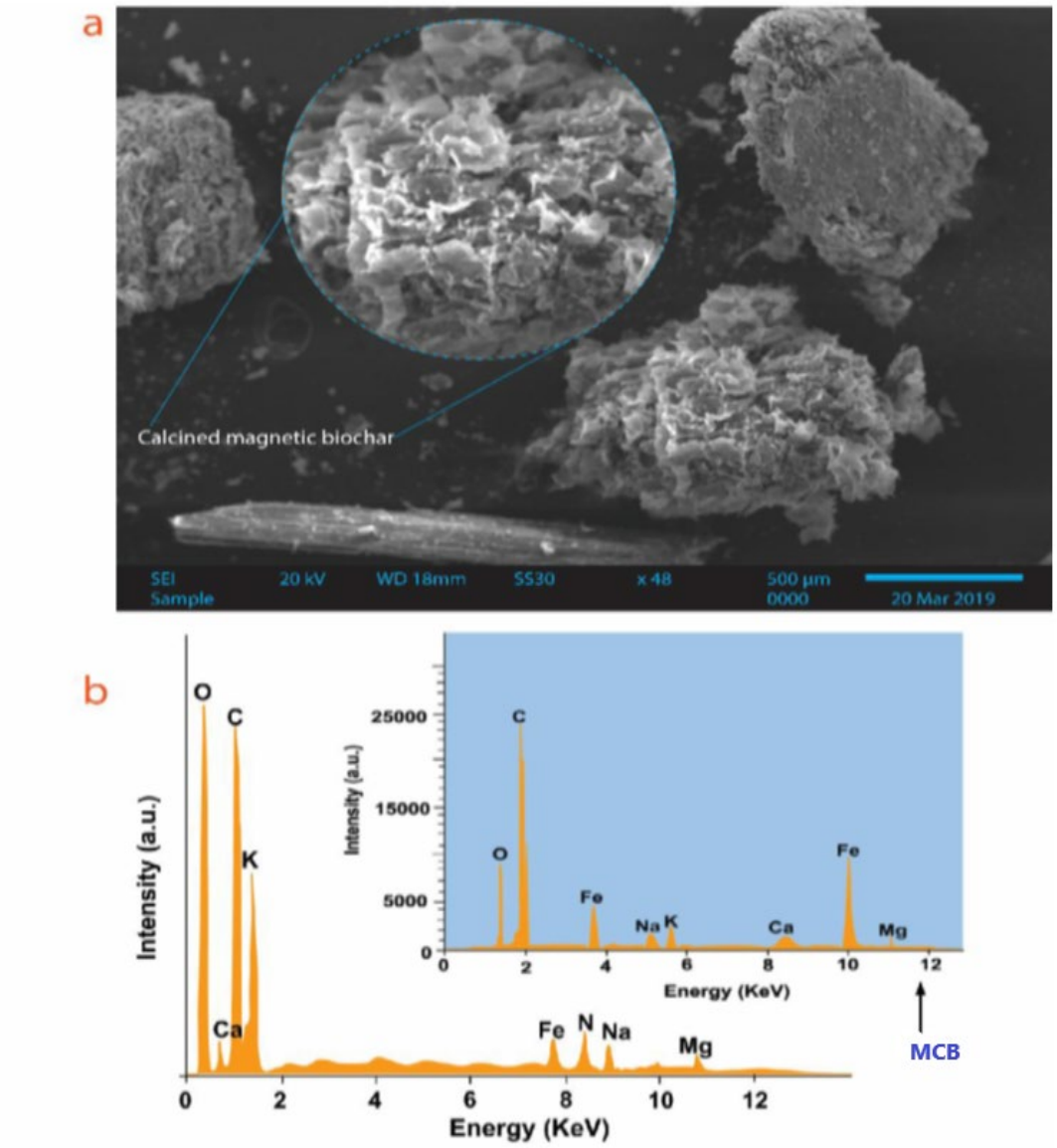

Figure 13: (a) SEM picture of MCB (inset) and CB. (b) Energy-dispersive X-ray of MCB (inset) and CB

4.2 Effects of adsorption parameters for pyrochar/AgBr

4.2.1 The influence of pH of 2,4,5-TCP

The effect of pH of 2,4,5-TCP was established via the batch adsorption system, where the solution pH was varied (2-10) with a constant dosage of 0.05 g pyrochar/AgBr, room temperature, and at a constant influent concentration (20 mg/L). Figure 14 shows that the magnitude of the 2,4,5-TCP adsorbed increased as the solution pH increased and the optimum adsorption occurred at pH 6, where the surface of the pyrochar/AgBr (pH_{pzc}=7.2) has more positively charged reactive sites, and the concentration of unionized 2,4,5-TCP species were high (solution pH < pKa (2,4,5-TCP pKa = 6.8)). Hence, dispersion interactions occurred between the unionized 2,4,5-TCP and the pyrochar/AgBr that is positively charged (Fan et al., 2011; Zango, Garba et al., 2016).

Note that the less uptake at pH 2 is attributed to the relatively lower quantity of the ionised 2,4,5-TCP compared to that at pH 6 (Zaghouane-Boudiaf & Boutahala, 2011). At alkaline conditions, when the solution pH > pKa, the unionized species of 2,4,5-TCP were lower than the ionized species, hence, electrostatic repulsions occurred between the negatively charged pyrochar/AgBr (pH_{pzc} < solution pH) and the chlorophenolate anions (Catherine et al., 2018; Gazi et al., 2017). Subsequently, a decreasing trend was noticed.

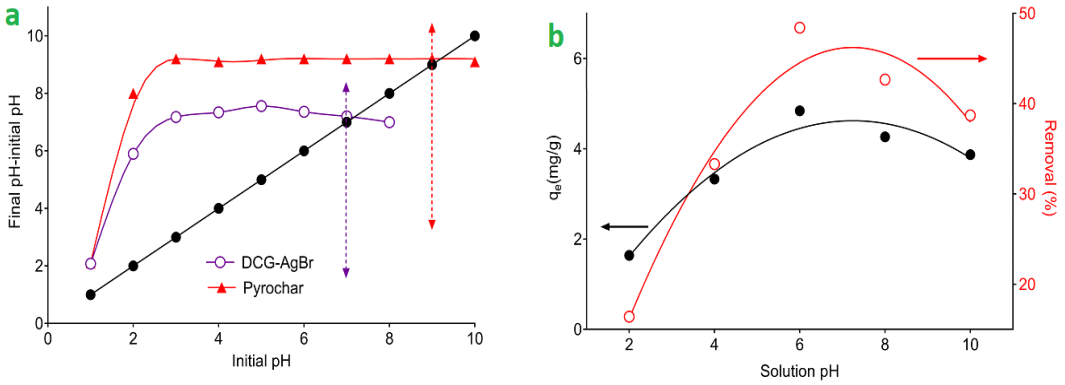

Figure 14: (a) pHpzc of the samples (b) batch system removal of 2,4,5-TCP under varying solution pH

4.2.2 The influence of influent rate of flow

Figure 15 displays the breakthrough curves at four varying rates of flow at a constant influent concentration (100 mg/L) and a bed height of 3 cm. Note that all the breakthrough curves reflect the regular curve that is S-shaped for the fixed-bed process. As the rate of flow increases from 1 mL/min to 10 mL/min before the bed became drenched, the service time and the magnitude effluent treated decreased proportionately also the slope of the S-shaped curve (dc/dt) decreases which indicates a shorter mass transfer zone (Δt) (Abdolali et al., 2017; Riazi et al., 2016). The faster rate flow provides insufficient residence time for mass transfer of 2,4,5-TCP into the pores of pyrochar/AgBr, thus, limiting the accessing of more active sites by the 2,4,5-TCP species within the pyrochar/AgBr (Oladipo & Gazi, 2016), consequently, lower removal efficiency was achieved. Also, note that the breakpoint and saturation time were delayed with a slower flow rate, suggesting effective intra-particle diffusion. Hence, the highest removal (84.5%) was attained at the least flow rate consistent with the reports from other researchers (Rao et al., 2011; Riazi et al., 2016).

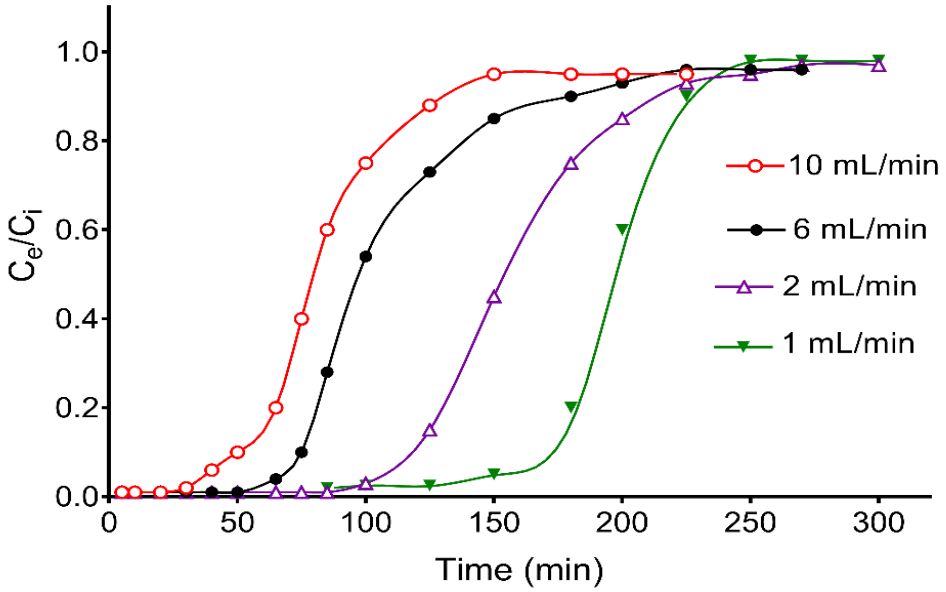

Figure 15: Influence of flow rate on breakthrough curve for 2,4,5-TCP adsorption by pyrochar/AgBr.

4.2.3 The influence of bed depth

Figure 16 shows the S-shaped curves of the 2,4,5-TCP adsorption onto pyrochar/AgBr at various bed depths (1– 3cm) corresponding to 1.5–4.5 g at a consistent rate flow (1 mL/min). As observed, the breakthrough time as well exhaustion time heightened obviously with more depths of bed. Specifically, the breakthrough occurred at 30, 50, 75 and 137 min for 1, 1.5, 2 and 3 cm bed depth, respectively ascribes to steeper breakthrough curves from mass transfer zone increase and the availability of higher active sites at higher bed depth (Golie & Upadhyayula, 2016). Note an increase in bed depth as the residence duration of 2,4,5-TCP inside the bed increased, enabling the deeper diffusion of the adsorbate species into the pyrochar/AgBr. Also, the removal performance heightened from 59.5% to ~86% from the predomination the mass transfer diffusion relative to the phenomenon of axial dispersion.

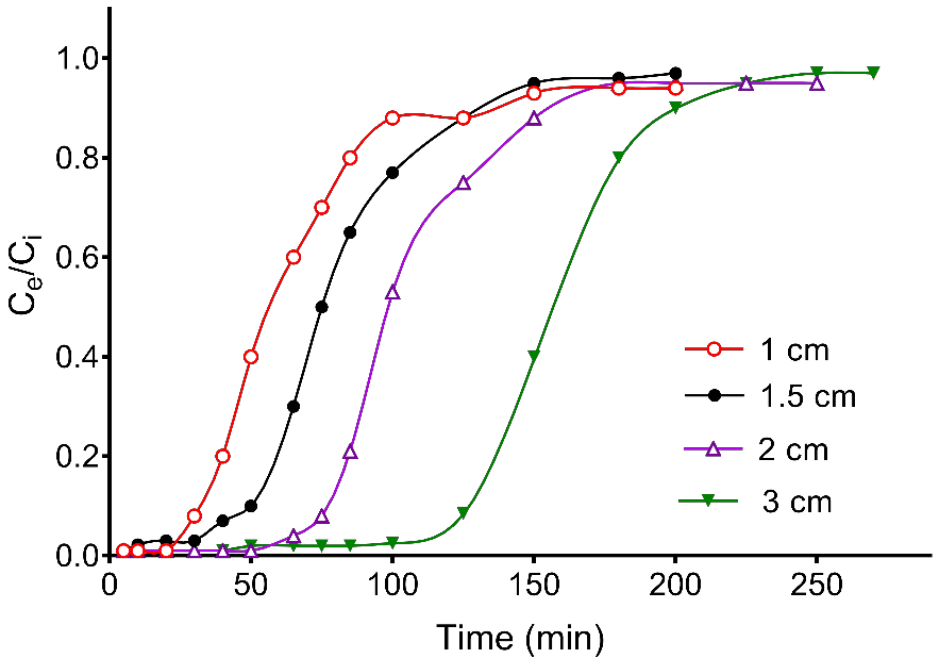

Figure 16: Effect of different bed depth in the adsorption of 2,4,5-TCP

4.2.4 Effect of inlet 2,4,5-TCP concentration

Figure 17 shows the breakthrough curves of 2,4,5-TCP adsorption at different inlet concentrations. Obviously, the saturation points became shorter and the breakthrough curves became sharper with an increase in concentration (20 to 100 mg/L). It was seen that the time for breakthrough was delayed when the pollutant concentration was decreased (Oladipo & Gazi, 2016; Gong et al., 2015). In particular, the saturation time was 80 min using a concentration of 100 mg/L increased to 195 min as influent concentration decreased to 20 mg/L. The removal performance was ~96% at 10 mg/L decreased to 85.5% as the influent concentration elevated to 100 mg/L. These results proved that lower initial concentration elongated the adsorption zone length and breakthrough time. At higher 2,4,5-TCP concentrations there is a higher concentration gradient and a lower mass transfer resistance (Jain et al., 2013; Zhu et al., 2017).

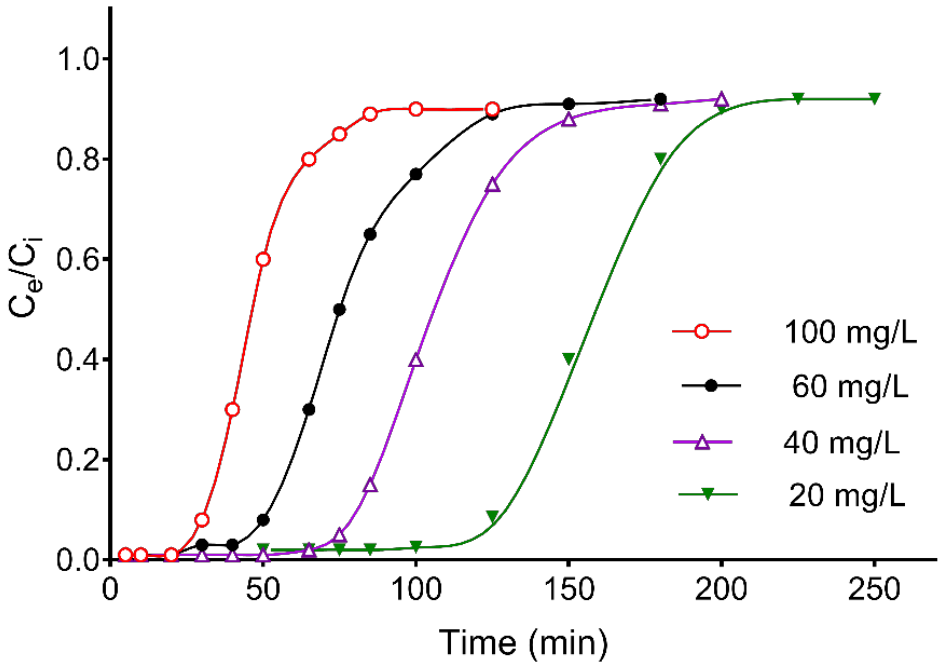

Figure 17: Influence of different influent concentrations on adsorption of 2,4,5-TCP.

4.3.5 The Effect of H_2O_2 concentration

The conduct of pyrochar/AgBr in the presence of an oxidizing reagent (H_2O_2) was investigated. Due to the high structural stabilization of the 2,4,5-TCP, it is believed that the oxidative cleavage of C-Cl in the 2,4,5-TCP can be achieved easily with existing hydroxyl radicals (•OH) (Gazi et al., 2017).

Here, the addition of H_2O_2 positively influenced 2,4,5-TCP removal. Specifically, at a 3 cm bed depth, the removal efficiency of pyrochar/AgBr obviously elevated from 75.5% to 97% as the influent concentration of H_2O_2 rose from 0.2 mM to 1 mM as shown in Figure 18. The pyrochar/AgBr acted as a Fenton-like catalyst and reacted with the H_2O_2 to produce oxidative species (•OH) (Oladipo et al., 2016) which caused oxidative cleavage of the of C-Cl. Nevertheless, the adsorption efficiency decreased to 81.2% as H_2O_2 concentration elevated beyond 1 Mm which is ascribed

to the scavenging effect of H_2O_2 towards the •OH radicals (Fida et al., 2017; Gazi et al., 2017).

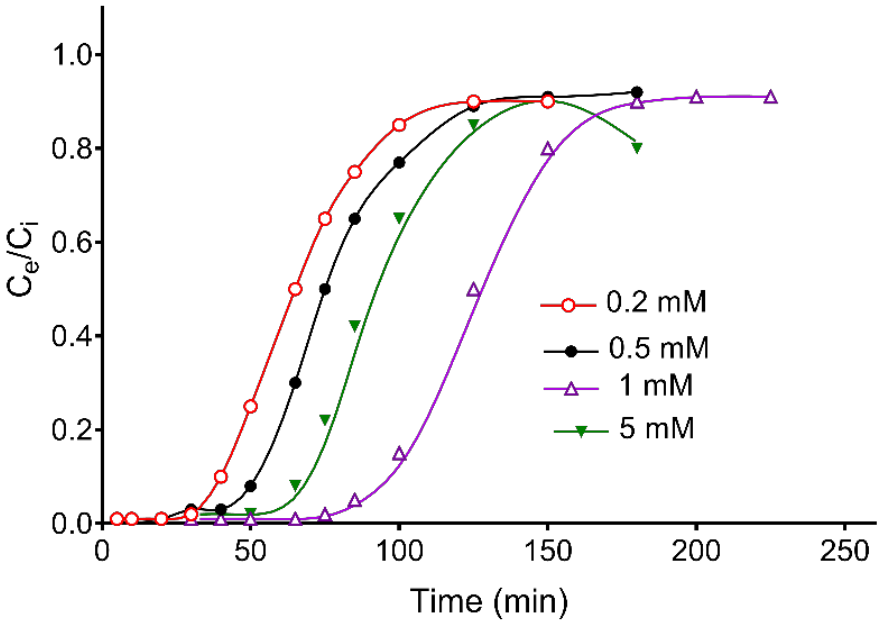

Figure 18: Influence of initial H_2O_2 concentration on breakthrough curve for 2,4,5-TCP adsorption.

4.4 Breakthrough curve modeling

Several models were adapted to decide the potent technique of the fixed-bed operations. The detailed description of the empirical models (Thomas, Clark, Bed Depth Service Time (BDST), Yoon-Nelson, Adams-Bohart, and Dose-response) have been reported (Oladipo & Gazi, 2014, 2016; Sivarajasekar et al., 2017). The evaluated parameters of the models obtained from the procedures data are listed in Table 8 and also Figure 19, at a bed depth (3 cm), constant influent concentration (10 mg/L), and varied flow rates. The most suitable model was selected based on the least average relative standard error (ARS), average relative error (ARE), and the highest correlation coefficient value (R^2). Based on the R^2 (0.997–0.999) values and the error function assessment (ARE = 1.34–2.45 and ARS= 2.11–2.59), the Thomas

model is considered the best suitable to explain the 2,4,5-TCP column adsorption followed by Yoon–Nelson model (ARE = 1.89–2.99 and ARS= 2.89–3.08). Notably, the dose–response model explains the breakthrough curves having a higher accuracy compared with the Clark, Adams– Bohart, and BDST models for the selected flow rates. The values of rate constant predicted by BDST model are consistent with that of Adams–Bohart model. However, the adsorption capacity data obtained by BDST model were slightly greater than that obtained of Adams–Bohart model, this could be attributed to the exclusion of the external film resistances and intraparticle mass transfer in the BDST for the indication of the adsorption capacity (Sivarajasekar et al., 2017). K_{YN} increased as the flow rate increases whereas for τ showed the trend was the reverse confirming that insufficient residence time and rapid exhaustion time occurred at a higher flow rate (Oladipo & Gazi, 2016).

4.5 Column desorption and reusability of pyrochar/AgBr

The desorption-regeneration-reuse of the pyrochar/AgBr in the column adsorption process was examined by successive recycle experiments. The outcome in **Figure 20** (inset) showed that 0.1 M NaOH was the best to be used to elute and effectively desorbed 96.2% of loaded 2,4,5-TCP compared with 35.9% achieved using 0.1 M HCl. The rate of dissolution of pyrochar/AgBr was rapid where ~88.5% 2,4,5-TCP was desorbed within the first 30 min which is comparable with the 99.4% 2,4,6-TCP desorbed from activated carbon (Fan et al., 2011). However, it took 24 h to achieve comparable per cent desorption in the presence of ethanol as the eluent. As shown in Figure 20, the desorbed pyrochar/AgBr was able to efficiently remove 2,4,5-TCP from the influent for up to 4 cycles with an adsorption efficiency of 89.7% after which, the adsorption zone decreased by 9% and slope of the breakthrough curve in the 5th cycle became narrower. As expected, the breakthrough and exhaustion time

were longer (t_b=100 min and t_e=175 min) for the first reuse cycle and decreased as the number of cycles increases.

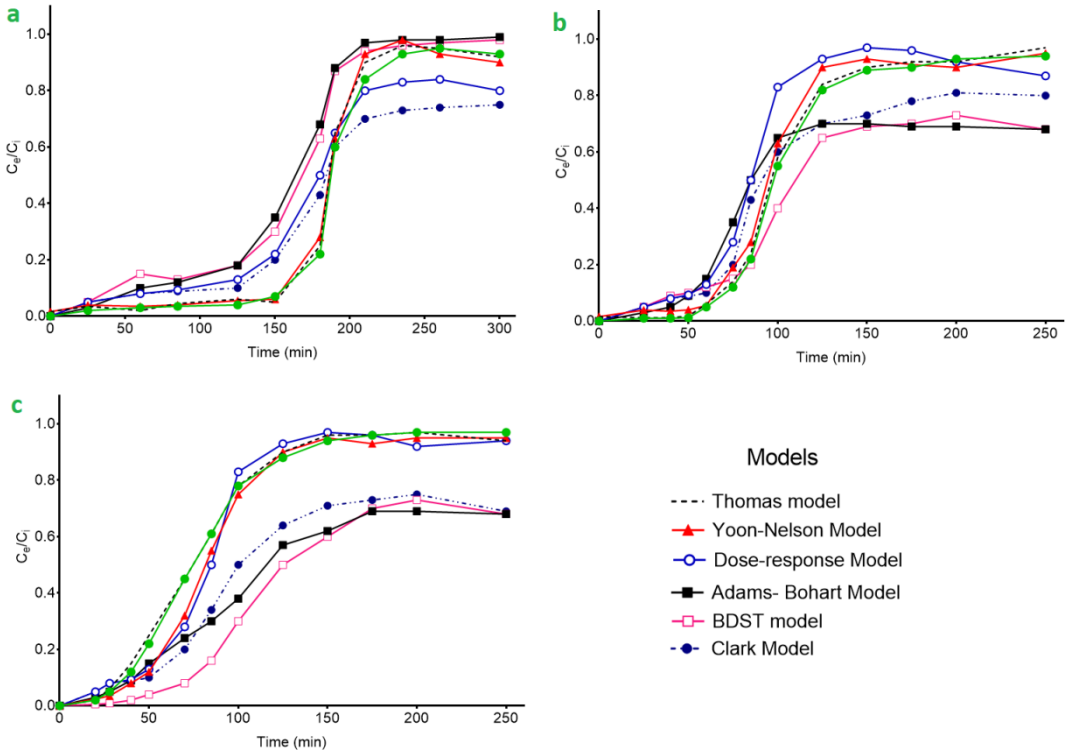

Figure 19: Breakthrough model curves at rate-flows (a) 1 mL/min, (b) 6 mL/min and (c) 10 mL/min for 2,4,5-TCP removal

Table 8: Characteristic parameters of various models at varying flow rates for 2,4,5-TCP removal

Model	Parameter	Flow rate		
Thomas		**1 mL/min**	**6 mL/min**	**10 mL/min**
	k_{TH} (mL/min)	0.122 ± 0.0016	0.039 ± 0.0012	0.077 ± 0.0011
	q_{TH} (mg/g)	67.3 ± 0.4	50.9 ± 0.8	38.6 ± 0.6
	ARE	1.34	2.23	2.45
	ARS	2.11	2.59	2.43
	R^2	0.997	0.999	0.998
Yoon-Nelson	K_{YN} (mL/min)	0.068	0.142	0.435
	τ (min)	68.5± 0.3	42.1± 0.6	33.8± 0.2
	ARE	1.03	2.88	2.66
	ARS	2.06	2.87	2.49
	R^2	0.997	0.999	0.998
BDST	k_{BDST} (L/mg min)	0.00029	0.00033	0.00042
	N_{BDST} (mg/L)	55.8± 0.6	50.7± 0.2	39.8± 0.9
	ARE	4.87	5.01	0.89
	ARS	6.32	1.89	5.07
	R^2	0.906	0.978	0.991
Adams-Bohart	K_{AB} (L/mg min)	0.00027	0.00035	0.00041
	N_{AB} (mg/L)	53.9± 0.2	49.3± 0.8	38.7± 0.3
	ARE	0.99	4.23	6.08
	ARS	5.17	6.33	4.02
	R^2	0.986	0.992	0.988
Dose-response	a_{DR}	4.13	5.74	5.88
	q_{DR} (mg/g)	26.89± 0.9	26.12± 0.3	25.89± 0.6
	ARE	0.89	3.21	3.66
	ARS	4.08	3.23	2.11
	R^2	0.993	0.994	0.997
Clark	N	0.967	0.908	0.997
	y_{CL} (1/min)	0.057	0.038	0.163
	J	3.20	11.9	56.9
	ARE	5.22	4.67	3.34
	ARS	8.45	6.77	4.78
	R^2	0.897	0.981	0.678

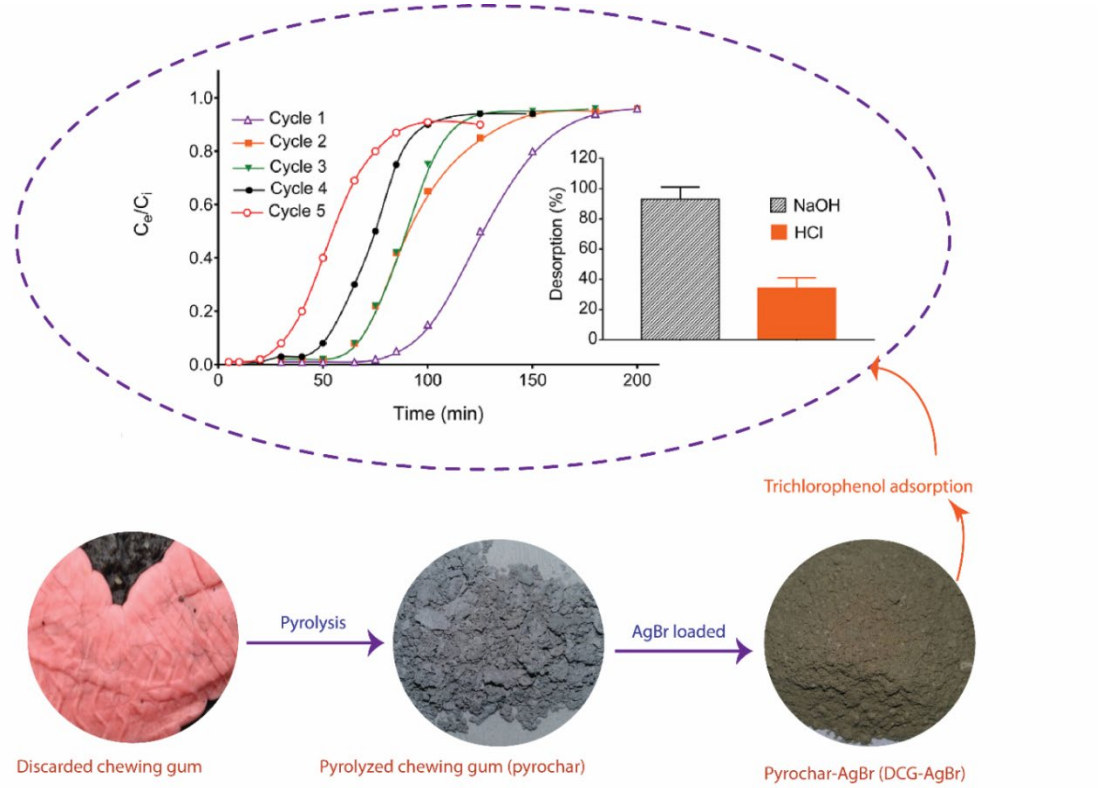

Figure 20: Adsorption-desorption breakthrough curves for the adsorption of 2,4,5-TCP (inset) cycles.

4.6 Effects of adsorption parameters for CB and MCB

4.6.1 The pH Effects on the efficiency of the MCB and CB

When the solution pH was altered from 2 to 10 the metal ions adsorption varied in like manner. MCB showed higher adsorption efficiencies as compared with CB in all instances. In Figure 21a, it shows MCB adsorbed almost 83% of Cu^{2+} at pH 4 and then at pH it increased to ~ 94% (37.6 and 47.9 mg/g for CB and MCB, respectively). The same trend was noticed for that of Zn^{2+} and Hg^{2+} adsorption where 76–85% removal capacity occurred at pH 4 and about 91–96% adsorption capacity at pH 6. The metal hydroxides formation at pH>6 attributes to its decreasing trend (Z. Ahmad et al., 2018). Although pH values at the end were higher than those began with as seen in Figure 21a as a result of the build-up of cations by the biochar during adsorption (Ahmad et al., 2018; Wang et al. 2015 DeMessie et al., 2015; Pap et al.

2018). Also, from then EDX, (Figure 12b) Mg^{2+}, K^{+}, and Ca^{2+} (0.045–0.068 mg/L) were observed and presumed to be released on the biochar surface.

The surface charge of the biochar at various pH and metal ions speciation explains trends observed. At pH < pH_{pzc} the adsorbents surface are positively charged and charged negatively at and pH > pH_{pzc}. The M (metal) species particularly existing in solution are M^{2+}, $M(OH)_2$ and MOH^{+} (Milenkovic et al., 2013) which all depend on the solution pH (Figure 21b–d). For lower pH values (< 4), the $M(OH)_2$ solubility is more; thus making, M^{2+} the prevalent species in the solution. At the pH range of greater than 4 to 9 the $M(OH)_2$ solubility decreases. For solution pH values >pH_{pzc}, there is electrostatic adsorption between the surface of MCB (negatively charged) and metal ion species (positively charged). Cu^{2+}, Zn^{2+}, and Hg^{2+} at pH 6 reached removal efficiencies of 91–96%. The removal efficiency remarkably decreased particularly for Cu^{2+} and Zn^{2+} when the pH further increases.

Generally, it is noticed that the uptake at pH 2–6 was a result of surface complexation of M^{2+} species with the adsorbent and/or biochar-π-cation interaction and not electrostatic interactions, while the electrostatic non-attraction that occurs between the biochars and $M(OH)_2$ decreased the metal adsorption at pH > 6.0.

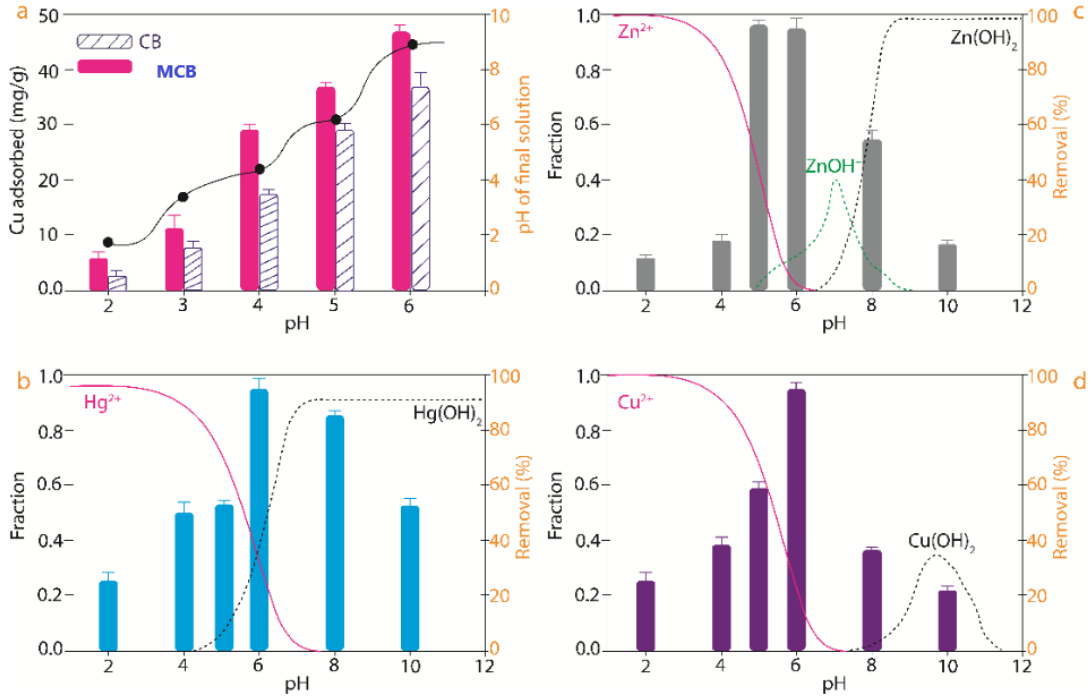

Figure 21: Influence of pH of solution on (a) adsorption of Cu^{2+} on MCB and CB (b, c, and d) adsorption of Hg^{2+}, Zn^{2+}, and Cu^{2+} respectively on MCB.

4.6.2 Effects of influent concentration and dosage on the efficiencies of the MCB and CB

Figure 22a–b shows that the removal capacity for Cu^{2+}, Zn^{2+}, and Hg^{2+} rapidly increased to 89–96% for both adsorbents with an increased dose of adsorbent till 0.2 g, while equilibrium was reached as the dosage approaches 0.5 g. The expanded surface area of the adsorbents resulting in increased functional groups, as well as more active sorption sites, explains the rapid uptake initially (Gazi et al., 2018). As against the initial rapid uptake a decrease in adsorption capacity was observed for both biochars which are attributed to concentration gradient of metal ion that is low and competition between incoming and adsorbed metal ions (Oladipo & Ifebajo, 2018; Tran et al., 2017). As the mass of MCB increases from 0.05 to 1.0 g the adsorption efficiencies at ~ 25 reduced to 1.2 mg per unit mass.

It is evident from Figure 22c–d that the metal ion concentration relatively increases with adsorption capacity as a result of a higher driving force (needed for the transportation of larger amounts of metal ion species to the reactive sites on the biochar) induced by the concentration gradient between the adsorbents and M^{2+}. Meanwhile, at added concentrations and constant dosage, the adsorption ability is lowered. There is an imbalance between the large magnitude of metal ions and the active adsorption sites available at higher concentrations; hence, removal efficiency decreases. The reverse is the case (higher removal efficiency) for concentrations lower, since the ratios of the M^{2+} to the available reactive sites in the solution are less.

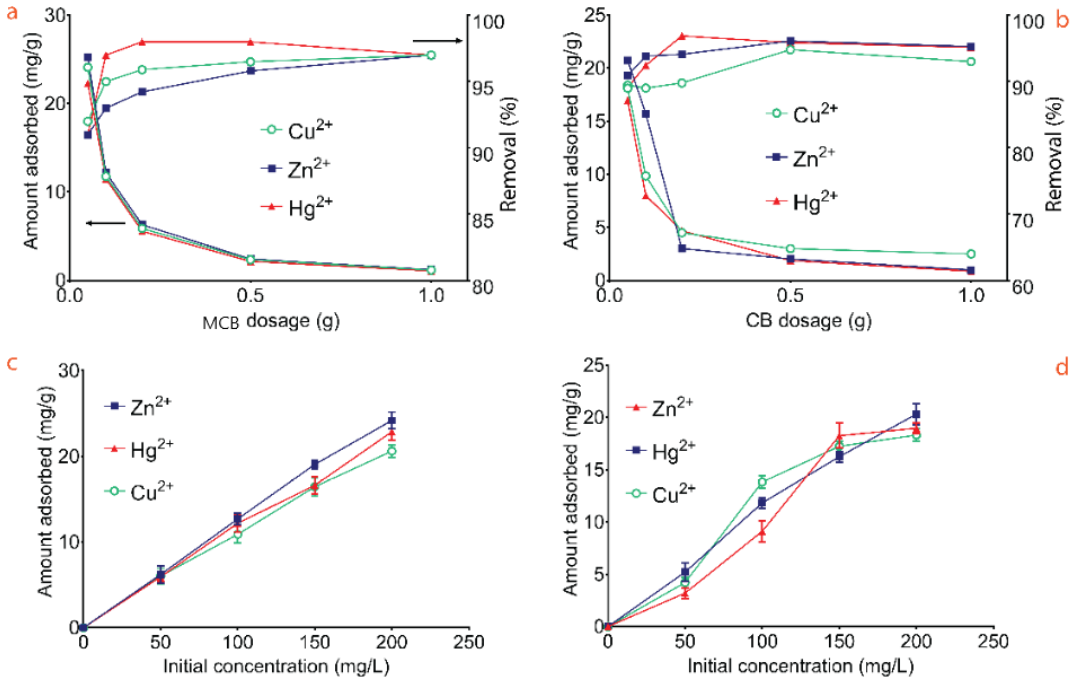

Figure 22: Effect of (a, b) dosage of adsorbent; and (c, d) initial metal concentration on the adsorption efficiencies of MCB and CB, respectively

4.7 Adsorption kinetics and isotherms

The rates of metal adsorption were observed to be higher on the magnetic calcined biochar (MCB) than the calcined biochar (CB) (Figure 23a–b). For both CB and MCB at pH 6, 25ºC, 100mg/L and 0.5 g dosage, the metal adsorption was swift at 0–60 min and then gradual till equilibrium is attained at 2 h. The swift uptake at the initial stages was possibly due to existing large magnitude of reactive sites on the biochar. But as the time advances the adsorption rate decreases until equilibrium was reached due to the contest on the saturated reactive sites. Thus, for subsequent experiments 2 h was selected as the duration for equilibrium.

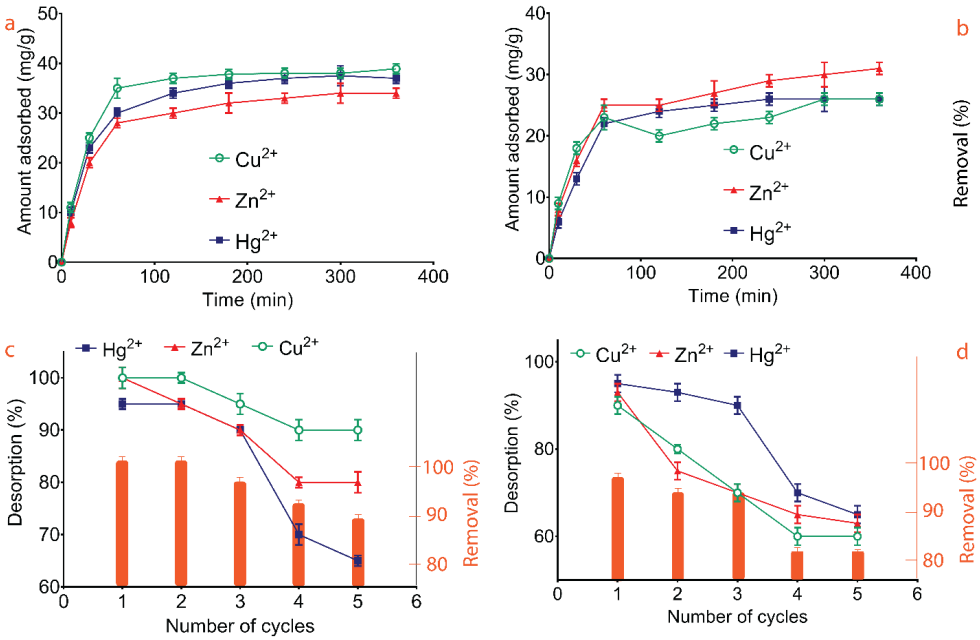

Figure 23: Effect of duration (a, b) on the sorption capacity of MCB and CB, respectively, and (c, d) desorption and regeneration of MCB and CB, respectively

To further study the mechanism of Zn^{2+}, Cu^{2+}, and Hg^{2+} adsorption on MCB and CB, Weber–Morris intra-particle diffusion models pseudo-second order, Elovich and pseudo-first order models were engaged to fit the parameters shown in **Table 9**. Looking at the R^2 values signifies that the adsorption processes are suitably fit for the

pseudo-second order equation ($R^2 > 0.994$). The differences (Δq_t) between the results obtained experimentally and the fitted equilibrium uptake capacities by pseudo-second order were lower in correlation to pseudo-first order. The adsorption, by assumptions of the pseudo-second order ensued by chemisorption interactions (Ho, 2006). Hence, the conclusion that the existence of a large number of surface acidic functional groups on the biochar is undoubtedly accountable for the adsorption.

To uphold the fact that the adsorption is through the chemisorption and surfaces are energetically heterogeneous are the higher values of R^2 (0.965–0.991) exhibited by the Elovich model in correlation to the pseudo-first order model (Oladipo & Gazi, 2015a, 2015b). The intraparticle diffusion model's relatively low error (χ = 0.5–1.9) and high R^2 values indicate that the metal ions diffusion from the solution into the porous biochar (Jia et al., 2019).

From the information in Table 10, it's obvious that the metal species concentration increase also increases the adsorption capacity. The experimental outcomes were correlated with the adsorption isotherms. Redlich-Peterson, Freundlich, and Langmuir isotherms were utilized where the correlation coefficient were higher for Langmuir and Redlich-Peterson isotherms (R^2 = 97.6–99.9%) than for the Freundlich isotherm (R^2 = 91.3–96.5%). This implies that no further interaction took place once the reactive sorption sites were occupied by the metal ions species (Pap et al., 2018; Selvanathan et al., 2017). The model tends toward monolayer adsorption which can be ascertained by the linearity constant "g" of the R-P isotherm at ~ 1.0 (Ahmad et al., 2018).

Table 9: Adsorption Kinetic parameters for the removal of metal ions by MCB and CB

			MCB			CB		
Kinetic models	**Equations**	**Parameters**	**Cu^{2+}**	**Zn^{2+}**	**Hg^{2+}**	**Cu^{2+}**	**Zn^{2+}**	**Hg^{2+}**
Elovich	$q_t = \frac{1}{\beta}\ln(\alpha\beta t + 1)$	$q_{e\ exp}$ (mg/g)	37.8	33.2	37.5	26.8	30.3	27.3
		α (mg/g min)	18.9	16.9	17.5	16.8	8.9	11.9
		β (g/mg)	4.8	5.3	5.9	6.3	11.4	6.4
		Δq_t	3.9	4.2	6.6	8.6	9.2	1.9
		R^2	0.965	0.969	0.971	0.991	0.991	0.989
		χ	0.08	0.23	0.56	0.66	3.2	1.8
Pseudo-second order	$q_t = \frac{k_2 q_e^2 t}{1 + k_2 q_e t}$	k_2 (g/mg min)	0.0034	0.0041	0.0025	0.0019	0.0036	0.0032
		$q_{e\ cal}$ (mg/g)	36.5	35.1	36.9	26.2	38.9	24.9
		Δq_t	1.3	1.9	0.6	0.6	8.6	2.4
		R^2	0.999	0.995	0.998	0.999	0.998	0.996
		χ	0.04	0.1	0.01	0.01	1.90	0.23
Pseudo-first order	$q_t = q_e(1 - e^{k_1 t})$	k_1 (1/ min)	0.0451	0.0434	0.0398	0.0288	0.0309	0.0298
		$q_{e\ cal}$ (mg/g)	17.9	23.1	27.8	10.9	15.4	16.9
		Δq_t	19.9	10.1	9.7	15.9	14.9	10.4
		R^2	0.865	0.911	0.899	0.969	0.933	0.789
		χ	1.11	4.42	3.38	23.19	14.42	6.4
Intra-particle difussion	$q_t = K_1 t^{1/2} + W$	k_p (mg/g $min^{0.5}$)	2.31	3.01	1.99	4.51	2.11	3.67
		C	10.9	13.3	11.2	19.3	9.8	15.5
		Δq_t	2.3	1.5	1.3	3.1	1.1	1.7
		R^2	0.993	0.989	0.988	0.996	0.983	0.992
		χ	0.5	1.4	1.9	0.9	1.60	1.8

Note $\chi = |q_{e,exp} - q_{e,cal}|/q_{e,cal}$

Table 10: Single-component adsorption isotherm parameters for the removal of metal ions

			MCB			CB		
Isotherms	**Equations**	**Parameters**	**Cu^{2+}**	**Zn^{2+}**	**Hg^{2+}**	**Cu^{2+}**	**Zn^{2+}**	**Hg^{2+}**
Freundlich	$q_e = K_F C_e{}^{1/n}$	k_F (mg/g)(mg/L)^n	12.9	12.6	13.5	11.8	11.5	10.6
		N	1.11	1.43	1.56	1.34	1.09	1.32
		Δq_e	8.8	8.3	9.2	6.9	7.4	8.9
		R^2	0.923	0.945	0.964	0.913	0.919	0.955
		χ	5.8	4.9	4.6	6.9	6.2	6.3
Langmuir	$q_e = \frac{q_m b C_e}{1 + b C_e}$	q_m (mg/g)	75.9	72.8	83.4	44.9	53.9	45.5
		b (L/mg)	11.5	9.1	12.9	8.2	7.5	10.3
		Δq_e	2.9	2.2	1.1	3.4	5.3	2.9
		R^2	0.976	0.989	0.999	0.999	0.989	0.994
		χ	1.2	1.8	3.1	1.9	3.4	2.3
Redlich-Peterson	$q_e = \frac{K_{rp} C_e}{1 + \alpha_{rp} C_e{}^{\beta}}$	K_{rp} (L/ g)	0.0782	0.0681	0.0599	0.0318	0.0399	0.0387
		α_{rp} (L/mg)^g	0.0034	0.0038	0.0041	0.0056	0.0062	0.0049
		Δq_e	2.8	2.5	1.4	3.2	4.9	2.8
		G	1.11	0.99	1.01	0.98	1.12	0.96
		R^2	0.993	0.998	0.999	0.988	0.995	0.996
		χ	1.11	4.42	3.38	23.19	14.42	6.40

Similarly, Pap et al., (2018) substantiated this conclusion where lead and Chromium were removed by the application of functionalized adsorbents sourced from fruit wastes. Clearly, the maximum adsorption capacity values (q_m) were higher for MCB ^{o}than CB in Langmuir isotherm and the adsorptions on heterogeneous surfaces were not applicable. Generally, the q_m of MCB proceeded in this order: Hg^{2+} (83.4 mg/g) > Cu^{2+} (75.9 mg/g) > Zn^{2+} (72.8 mg/g), whereas that of CB is Zn^{2+} (53.9 mg/g) > Hg^{2+} (45.5 mg/g) > Cu2+ (44.9 mg/g).

4.8 Thermodynamics parameters

The adsorption thermodynamics were also evaluated and the thermodynamic parameters which include; Gibb's free energy (ΔG^o), change in entopy (ΔS^o), and change in enthalpy (ΔH^o) for the adsorption of the heavy metals unto CB and MCB using the equations (8), (9), and (10).

$$\Delta\ ^{o} = -RT \ln k \quad (8)$$

$$\Delta\ ^{o} = \Delta H^{o} - T\Delta S^{o} \quad (9)$$

$$\ln K = -{}^{\Delta H}/_{RT} + {}^{\Delta S}/_{R} \quad (10)$$

Where R (J mol^{-1} K^{-1}) is the gas constant, T (K) is the temperature and K is the equilibrium constant. Linear plot of In K versus 1/T gives the slop and intercept which provides the value of ΔH° and ΔS°, respectively as shown in (10).

Table 11: Coefficients of adsorption thermodynamics

			ΔG^o (kJ/mol)		
CB	**ΔH° (kJ/mol)**	**ΔS° (J/mol)**	**298 K**	**313K**	**338K**
Cu^{2+}	-270.80	-50.11	-3.85	-2.92	-1.83
Hg^{2+}	-373.18	-76.39	-3.43	-.120	-0.28
Zn^{2+}	-135.73	-22.24	-2.78	-2.37	-1.88
MCB					
Cu^{2+}	-416.47	-85.17	-3.85	-1.36	-0.34
Hg^{2+}	-128.91	-28.98	-0.42	0.40	0.77
Zn^{2+}	-118.73	-20.22	-2.26	-1.75	-1.43

Generally, the values of ΔG^0 were negative at all temperatures and the negative values confirm the feasibility of the process and the spontaneous nature of heavy metals adsorption onto treated CB amd MCB although for Hg^{2+} at 40^o C and 65^o C the values are positive indicating non-spontaneity of reaction.the magnitude of ΔG^o gives an idea about the nature of adsorption process.from the Table 11 it is observed that the ΔG^o values falls in the range of -20 to 0 kJ/mol indicating a physisorption (Oladipo & Gazi, 2014). The negative values of ΔH^o for the metal adsorption reflects an exothermic reaction. Also the negative entopy values means that the degree of system chaos decreased because the heavy metals were adsorbed ontothe adsorbents.

4.8 Competitive/multicomponent adsorption

The selective adsorption of MCB from a multicomponent solution was also examined and the outcome obtained from experiments suited to the extended Langmuir equation (Oladipo & Gazi, 2015b; Oladipo et al., 2015). As expected, the quantity of Cu^{2+}, Zn^{2+}, and Hg^{2+} adsorbed from the competitive adsorption is lower than their corresponding uptakes in the single-component system. Particularly, at 20 mg/L concentration for each metal ion in the multi-component system, a reduction of 56.9, 58.9, and 35.8% for Cu^{2+}, Zn^{2+}, and Hg^{2+}, respectively was recorded (Table 12). To explain the effect of interference, β (a selectivity factor) was brought in for increases in the concentration of each component metal ion. The order for MCB adsorption dynamics in the multi-component solution proceeds as thus: $Hg^{2+} > Cu^{2+} > Zn^{2+}$. The metal ion selectivity and the competitive adsorption in a multi-component system are affected by factors like charge density, electronegativity of metal, hydrated ions radii, and size of the metal ions (Ahmad et al., 2018; Cutillas-Barreiro et al., 2016; Ding et al., 2016). Metal ions investigated here possess similar charges; thus, the selectivity was possibly determined by their electronegativity and

ionic radius. Hg^{2+}, Cu^{2+}, and Zn^{2+} ionic radius are 110, 74, and 71 p.m., respectively while their electronegativities are 2.0, 1.9,and1.65 accordingly. This explains why Hg^{2+} will be adsorbed preferentially in the existence of Zn^{2+} and Cu^{2+}.

Notice that in the existence of a relatively high concentration of Hg^{2+} (20 mg/L) an important reduction was observed in the adsorption of Cu^{2+}. This differs at lower concentrations Hg^{2+} (10 mg/L) where an opposing influence of Hg^{2+} approaching Cu^{2+} removal in a multicomponent system thus the adsorption of Cu^{2+} was slightly inhibited (Table 12). This proves the fact that the adsorption of Hg^{2+} is improved by its selectivity towards MCB that is positively charged as a result of its relatively high electronegativity and less hydrated ionic radius.

Table 12: Competitive adsorption parameters for the removal of metal ions

Multi-component isotherm analysis for competitive metal ion adsorption by MCB								
System	**Concentration (mg/L)**			**Extended Langmuir adsorption isotherm parameters***				
	$C_{o,Cu}$	$C_{o,Zn}$	$C_{o,Hg}$	q_m (mg/g)	N	β	R^2	χ
Cu^{2+}-ternary	20	20	20	32.7	2.11	2.67	0.996	1.45
	20	10	20	38.9	3.91	1.98	0.987	2.11
	10	10	10	69.5	3.19	0.89	0.989	6.12
Zn^{2+}-ternary	10	10	10	19.6	2.87	1.67	0.999	4.89
	20	20	20	29.9	1.89	2.09	0.997	5.44
	10	20	10	45.8	3.89	2.87	1.000	9.11
Hg^{2+}-ternary	20	20	10	42.5	2.24	2.99	0.989	6.89
	10	10	20	49.5	3.37	3.15	0.999	7.33
	20	20	20	53.5	4.01	3.55	0.988	8.96

4.9 Desorption and regenerative efficiency of spent adsorbents

The adsorbents loaded with heavy metal ions were desorbed using distilled water spiked with 0.1 M NaOH and agitated. The desorbed biochars were overnight dried

at 60 °C, and then utilized for 5 successive cycles. 91–100% Cu^{2+} was desorbed from MCB within the five consecutive cycles as against the trend observed for CB (Figure 23c–d). The bars in Figure 23c–d indicates that the first reuse for Cu^{2+} removal was ~ 97% but decreased to 89% in the fifth reuse for MCB, while that for CB at the fifth cycle was 82%. It's important to note that at the fifth regenerative cycle, the structural features of the adsorbents were intact, suggesting efficiency and outstanding regenerative-ability of the as-fabricated biochars.

4.10 Insights to adsorption Mechanism

Taking into account the charge on the surface of the adsorbents and the metal ions species, it is obvious that the interaction (biochar-π–cation) and/or surface complexation of metal ion species with the biochar determine the adsorption at the solution pH of 2–6. Electrostatic attraction occurs at pH > 6, between the biochar (negatively charged) and metal ions (positively charged). The discharge of alkaline mineral ash on the surface of biochar accounts for the pH solution increase.

XRD and FTIR characterizations were also carried out after adsorption to analyse the surface compositions and structural features of the M^{2+}–loaded biochar. The C=O vibration bonds (1573 cm^{-1}) were no longer visible. The peaks at 525 cm^{-1} (Fe-O) and 3048 cm^{-1} (-OH) drastically reduced in intensity shifting to 510 and 3029 cm^{-1} respectively in MCB spectrum indicating an oxygen-metal stretching (i.e., Cu /Zn/ Hg /Fe-O stretching). The electrostatic metal ion–π interactions is validated by the reduction in peaks at 678 and 774 cm^{-1} assigned to graphite structure (Sizmur et al., 2017). The total pore volume and S_{BET} of MCB reduced from 0.34 to 0.12 cm^3 /g and from 323.2 to 259.7 m^2 /g respectively. Also, the XRD peaks of MCB also weakened after the adsorption of metal ions.

Nonetheless, the textural integrity of the M^{2+}-loaded biochar was intact. The characterization results conclude that ion exchange, inner-sphere surface complexation, and M^{2+}-π electrostatic interaction controls the single-component adsorption system while hydration energy, size, and electronegativity value governs the selectivity of metal ion in the multi-metal system. Figure 24 illustrates the mechanism by which metal ions are removed by (MCB) taking into account adsorption trends and results obtained in this work.

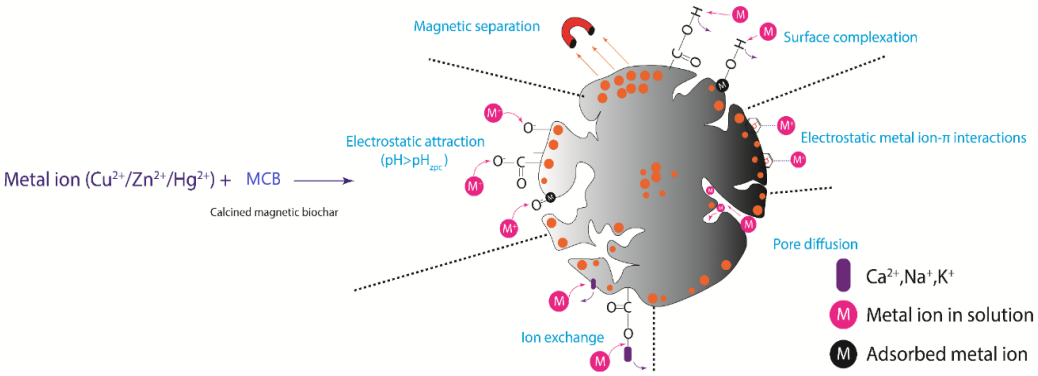

Figure 24: Uptake mechanism of metal ions by MCB

4.11 Economic analysis for treatment of 2,4,5-TCP simulated wastewater

Majorly taking into consideration the cost of electricity and costs of preparing pyrochar/AgBr, eluent (NaOH) an economic analysis was evaluated. From the electricity tariff of Northern Cyprus (April 2019) and Chemicals from Sigma-Aldrich (Germany), electricity cost is 2.2 US$ per 100 kW, pyrochar/AgBr and NaOH are 9.5 and 33.5 US$/kg respectively. Cost of the fixed-bed column operation for removal of 2,4,5- TCP is estimated from this work looking at the optimum treatment parameters (pH 6, influent concentration: 10 mg/L, NaOH eluent: 0.1 M,

fixed removal efficiency of 96%). The power consumption for the 12 h treatment of 2,4,5-TCP (0.25 m^3) simulated water was obtained as 13.3 kW. As a result, the adsorbent and eluent costs for this process are 1.17 US$/$m^3$, 19 US$ and 6.89 US$, respectively. Subsequently, the total treatment cost of 2,4,5-TCP simulated wastewater via the fixed-bed system was 27.06 US$/$m^3$. Considering the reusability potential of pyrochar/AgBr and its high performance during the five successive regenerative cycles, the cost of pyrochar/AgBr was reduced by 3. Hence, the total cost was estimated to be 14.39 US$/$m^3$. The economic analyses demonstrated that the treatment technology discussed here is promising and can be improved for industrial-scale treatment of phenolic contaminated wastewaters.

Table 13: General summary of work

Adsorbent	**Calcined Biochar CB**	**Magnetic Calcined Biochar MCB**	**Pyrochar/AgBr**
Source Material	Banana peels	Banana peels	Discarded chewing gum
Characterization	FTIR	FTIR	FTIR
	BET	BET	BET
	SEM	Specific saturation magnetization	SEM
	XRD	SEM	EDX
	EDX	EDX	
Pollutants removed	Cu^{2+}, Zn^{2+}, Hg^{2+}	Cu^{2+}, Zn^{2+}, Hg^{2+}	2,4,5- TCP
Maximum adsorption (mg/g)	44.9, 53.9, 45.5	75.9, 72.9, 83.4	67.3 ± 4
Adsorption mechanism	Pseudo-second order Langmuir Model	Pseudo-second order Langmuir Model	Thomas model

Chapter 5

CONCLUSION

In summary, effective, alternative low-cost adsorbents can be produced from saccharides for the elimination of contaminants from wastewater. Calcined biochar (CB) and its magnetic derivative (MCB) were readily produced using banana peels as an economic source for the removal of Cu^{2+}, Hg^{2+}, and Zn^{2+} ions while pyrochar/AgBr prepared from discarded chewing gum was used effectively for decontaminating trichlorophenols from simulated solutions (aqueous). The evaluation of the experimental results unveils the following:

- Both biochars (MCB and CB) possessed an excellent efficiency for metal ion adsorption, as a result of its porosity (which is a mixture of mesopores and micropores), comparatively high S_{BET} (95.9–323.2 m^2 /g), and the existence of large number of surface oxygen-containing functionalities (–OH and –COO–)
- For the single-component system, the adsorption of metal ions species onto CB and MCB was controlled by ion exchange, inner-sphere surface complexation, and M^{2+}-π electrostatic interaction
- Optimum adsorption capacities of MCB according to Langmuir were 72.8, 75.9, and 83.4 mg/g for Zn^{2+}, Cu^{2+}, and Hg^{2+}, respectively
- Hg^{2+} significantly inhibited the removal of Cu^{2+} in multicomponent systems
- Banana peel–based biochar has the potentials to be applied as a tenable and potent adsorbent for removal of metal ions from wastewater.

- In the fixed-bed mode, the maximum 2,4,5- TCP uptake was 29.9 mg/g at a bed depth 3 cm, an influent concentration of 100 mg/L, and 1 mL/min rate-flow
- The pyrochar–AgBr maintained stable regeneration-reuse activity for at least 5 cycles without significant loss of performance
- Desorption studies confirmed that it was possible to desorb ~96% of loaded 2,4,5-TCP using 0.01 M NaOH solution.
- Yoon–Nelson Thomas models are evidently suitable to evaluate the S-shaped (breakthrough) curves of the 2,4,5-TCP adsorption process.

REFERENCES

Abdolali, A., Ngo, H. H., Guo, W. S., Zhou, J. L., Zhang, J., Liang, S., et al. (2017). Application of a breakthrough biosorbent for removing heavy metals from synthetic and real wastewaters in a lab-scale continuous fixed-bed column. *Bioresource Technology, 229*, 78-87.

Ahmad, T., & Danish, M. (2018). Prospects of banana waste utilization in wastewater treatment: A review. *Journal of Environmental Management, 206*, 330-348.

Ahmad, T., Rafatullah, M., Ghazali, A., Sulaiman, O., Hashim, R., & Ahmad, A. (2010). Removal of Pesticides from Water and Wastewater by Different Adsorbents: A Review. *Journal of Environmental Science and Health Part C-Environmental Carcinogenesis & Ecotoxicology Reviews, 28*(4), 231-271.

Ahmad, Z., Gao, B., Mosa, A., Yu, H. W., Yin, X. Q., Bashir, A., et al. (2018). Removal of Cu(II), Cd(II) and Pb(II) ions from aqueous solutions by biochars derived from potassium-rich biomass. *Journal of Cleaner Production, 180*, 437-449.

Ahmed, S., Rasul, M. G., Martens, W. N., Brown, R., & Hashib, M. A. (2011). Advances in Heterogeneous Photocatalytic Degradation of Phenols and Dyes in Wastewater: A Review. *Water Air and Soil Pollution, 215*(1-4), 3-29.

Akpor, B. O., Onolunose., O. G., & Tomilola., O. D. (2014). Heavy metal pollutants in wastewater effluents: Sources, effects and remediation. *Advances in Bioscience and Bioengineering, 2*(4), 37-43.

Alguacil, F. J. (2019). The removal of toxic metals from liquid effluents by ion exchange resins. Part IX: Lead(II)/H plus /Amberlite IR-120. *Revista De Metalurgia, 55*(1).

Ali, A., & Saeed, K. (2016). Phenol removal from aqueous medium using chemically modified banana peels as low-cost adsorbent. *Desalination and Water Treatment, 57*(24), 11242-11254.

Alves, C. C. O., Franca, A. S., & Oliveira, L. S. (2013). Evaluation of an Adsorbent Based on Agricultural Waste (Corn Cobs) for Removal of Tyrosine and Phenylalanine from Aqueous Solutions. *Biomed Research International*, 2013, 1-8.

Amin, M. T., Alazba, A. A., & Manzoor, U. (2014). A Review of Removal of Pollutants from Water/Wastewater Using Different Types of Nanomaterials. *Advances in Materials Science and Engineering,* 2014, 1-24.

Awad, A. M., Shaikh, S. M. R., Jalab, R., Gulied, M. H., Nasser, M. S., Benamor, A., et al. (2019). Adsorption of organic pollutants by natural and modified clays: A comprehensive review. *Separation and Purification Technology, 228*.

Ayala, J., & Fernandez, B. (2019). Treatment of mining waste leachate by the adsorption process using spent coffee grounds. *Environmental Technology, 40*(15), 2037-2051.

Barakat, M. A. (2011). New trends in removing heavy metals from industrial wastewater. *Arabian Journal of Chemistry, 4*(4), 361-377.

Bhatnagar, A., Sillanpaa, M., & Witek-Krowiak, A. (2015). Agricultural waste peels as versatile biomass for water purification - A review. *Chemical Engineering Journal, 270*, 244-271.

Bibaj, E., Lysigaki, K., Nolan, J. W., Seyedsalehi, M., Deliyanni, E. A., Mitropoulos, A. C., et al. (2019). Activated carbons from banana peels for the removal of nickel ions. *International Journal of Environmental Science and Technology, 16*(2), 667-680.

Blackburn, R. S. (2004). Natural polysaccharides and their interactions with dye molecules: Applications in effluent treatment. *Environmental Science & Technology, 38*(18), 4905-4909.

Busca, G., Berardinelli, S., Resini, C., & Arrighi, L. (2008). Technologies for the removal of phenol from fluid streams: A short review of recent developments. *Journal of Hazardous Materials, 160*(2-3), 265-288.

Castro, R. S. D., Caetano, L., Ferreira, G., Padilha, P. M., Saeki, M. J., Zara, L. F., et al. (2011). Banana Peel Applied to the Solid Phase Extraction of Copper and

Lead from River Water: Preconcentration of Metal Ions with a Fruit Waste. *Industrial & Engineering Chemistry Research, 50*(6), 3446-3451.

Catherine, H. N., Ou, M. H., Manu, B., & Shih, Y. H. (2018). Adsorption mechanism of emerging and conventional phenolic compounds on graphene oxide nanoflakes in water. *Science of the Total Environment, 635*, 629-638.

Crini, G. (2005). Recent developments in polysaccharide-based materials used as adsorbents in wastewater treatment. *Progress in Polymer Science, 30*(1), 38-70.

Crini, G., & Lichtfouse, E. (2019). Advantages and disadvantages of techniques used for wastewater treatment. *Environmental Chemistry Letters, 17*(1), 145-155.

Cutillas-Barreiro, L., Paradelo, R., Igrexas-Soto, A., Nunez-Delgado, A., Fernandez-Sanjurjo, M. J., Alvarez-Rodriguez, E., et al. (2016). Valorization of biosorbent obtained from a forestry waste: Competitive adsorption, desorption and transport of Cd, Cu, Ni, Pb and Zn. *Ecotoxicology and Environmental Safety, 131*, 118-126.

De Gisi, S., Lofrano, G., Grassi, M., & Notarnicola, M. (2016). Characteristics and adsorption capacities of low-cost sorbents for wastewater treatment: A

review. *Sustainable Materials and Technology, 9*, 10-40.

DeMessie, B., Sahle-Demessie, E., & Sorial, G. A. (2015). Cleaning Water Contaminated with Heavy Metal Ions Using Pyrolyzed Biochar Adsorbents. *Separation Science and Technology, 50*(16), 2448-2457.

Deng, Y., & Zhao, R. Z. (2015). Advanced Oxidation Processes (AOPs) in Wastewater Treatment. *Current Pollution Reports, 1*(3), 167-176.

Dichiara, A. B., Weinstein, S. J., & Rogers, R. E. (2015). On the Choice of Batch or Fixed Bed Adsorption Processes for Wastewater Treatment. *Industrial & Engineering Chemistry Research, 54*(34), 8579-8586.

Ding, Y., Liu, Y. G., Liu, S. B., Li, Z. W., Tan, X. F., Huang, X. X., et al. (2016). Competitive removal of Cd(II) and Pb(II) by biochars produced from water hyacinths: performance and mechanism. *Rsc Advances, 6*(7), 5223-5232.

Dragani, R. (2019). What Effects Does Bubble Gum Have on the Environment? Retrieved from https://sciencing.com/pumice-powder-used-for-5900703.html

El-Din, G. A., Amer, A. A., Malsh, G., & Hussein, M. (2018). Study on the use of banana peels for oil spill removal. *Alexandria Engineering Journal, 57*(3), 2061-2068.

Faheem, Yu, H. X., Liu, J., Shen, J. Y., Sun, X. Y., Li, J. S., et al. (2016). Preparation of MnOx-loaded biochar for Pb2+ removal: Adsorption performance and possible mechanism. *Journal of the Taiwan Institute of Chemical Engineers, 66*, 313-320.

Fan, J. L., Zhang, J., Zhang, C. L., Ren, L. A., & Shi, Q. Q. (2011). Adsorption of 2,4,6-trichlorophenol from aqueous solution onto activated carbon derived from loosestrife. *Desalination, 267*(2-3), 139-146.

Farooq, U., Kozinski, J. A., Khan, M. A., & Athar, M. (2010). Biosorption of heavy metal ions using wheat based biosorbents - A review of the recent literature. *Bioresource Technology, 101*(14), 5043-5053.

Fida, H., Zhang, G., Guo, S., & Naeem, A. (2017). Heterogeneous Fenton degradation of organic dyes in batch and fixed bed using La-Fe montmorillonite as catalyst. *Journal of Colloid and Interface Science, 490*, 859-868.

Gazi, M., Oladipo, A. A., & Azalok, K. A. (2018). Highly efficient and magnetically separable palm seed-based biochar for the removal of nickel. *Separation Science and Technology, 53*(7), 1124-1131.

Gazi, M., Oladipo, A. A., Ojoro, Z. E., & Gulcan, H. O. (2017). High-Performance Nanocatalyst for Adsorptive and Photo-Assisted Fenton-Like Degradation of Phenol: Modeling Using Artificial Neural Networks. *Chemical Engineering Communications, 204*(7), 729-738.

Golie, W. M., & Upadhyayula, S. (2016). Continuous fixed-bed column study for the removal of nitrate from water using chitosan/alumina composite. *Journal of Water Process Engineering, 12*, 58-65.

Gong, J. L., Zhang, Y. L., Jiang, Y., Zeng, G. M., Cui, Z. H., Liu, K., et al. (2015). Continuous adsorption of Pb(II) and methylene blue by engineered graphite oxide coated sand in fixed-bed column. *Applied Surface Science, 330*, 148-157.

Gupta, V. K., Carrott, P. J., Suhas., & Carrott, M. L. (2009). Low-Cost Adsorbents: Growing Approach to Wastewater Treatment - a Review. *Critical Reviews in Environmental Science and Technology, 39*(10), 783-842.

Gupta, V. K., Carrott, P. J. M., Carrott, M., & Suhas. (2009). Low-Cost Adsorbents: Growing Approach to Wastewater Treatmenta Review. *Critical Reviews in Environmental Science and Technology, 39*(10), 783-842.

Hegazi, H. A. (2013). Removal of heavy metals from wastewater using agricultural and industrial wastes as adsorbents. *HBRC Journal, 9*(3), 276-282.

Ho, Y. S. (2006). Review of second-order models for adsorption systems. *Journal of Hazardous Materials, 136*(3), 681-689.

Ifebajo, A. O., Oladipo, A. A., & Gazi, M. (2019). Efficient removal of tetracycline by CoO/CuFe2O4 derived from layered double hydroxides. *Environmental Chemistry Letters, 17*(1), 487-494.

Inyang, M. I., Gao, B., Yao, Y., Xue, Y. W., Zimmerman, A., Mosa, A., et al. (2016). A review of biochar as a low-cost adsorbent for aqueous heavy metal

removal. *Critical Reviews in Environmental Science and Technology, 46*(4), 406-433.

Jain, M., Garg, V. K., & Kadirvelu, K. (2013). Cadmium(II) sorption and desorption in a fixed bed column using sunflower waste carbon calcium-alginate beads. *Bioresource Technology, 129*, 242-248.

Jaria, G., Silva, C. P., Oliveira, J., Santos, S. M., Gil, M. V., Otero, M., et al. (2019). Production of highly efficient activated carbons from industrial wastes for the removal of pharmaceuticals from water-A full factorial design. *Journal of Hazardous Materials, 370*, 212-218.

Jia, Y., Zhang, Y. S., Fu, J. G., Yuan, L. X., Li, Z., Liu, C., et al. (2019). A novel magnetic biochar/MgFe-layered double hydroxides composite removing Pb2+ from aqueous solution: Isotherms, kinetics and thermodynamics. *Colloids and Surfaces a-Physicochemical and Engineering Aspects, 567*, 278-287.

Jiang, R. X., Tian, J. Y., Zheng, H., Qi, J. Q., Sun, S. J., & Li, X. C. (2015). A novel magnetic adsorbent based on waste litchi peels for removing Pb(II) from aqueous solution. *Journal of Environmental Management, 155*, 24-30.

Joshiba, G. J., Kumar, P. S., Femina, C. C., Jayashree, E., Racchana, R., & Sivanesan, S. (2019). Critical review on biological treatment strategies of dairy wastewater. *Desalination and Water Treatment, 160*, 94-109.

Kanaujiya, D. K., Paul, T., Sinharoy, A., & Pakshirajan, K. (2019). Biological Treatment Processes for the Removal of Organic Micropollutants from Wastewater: a Review. *Current Pollution Reports, 5*(3), 112-128.

Kansara, N., Bhati, L., Narang, M., & Vaishnavi, R. (2016). Wastewater treatment by ion exchange method: a review of past and recent researches. *Environmental Science an Indian Journal, 12*(4), 143-150.

Kapur, M., & Mondal, M. K. (2016). Design and model parameters estimation for fixed-bed column adsorption of Cu(II) and Ni(II) ions using magnetized saw dust. *Desalination and Water Treatment, 57*(26), 12192-12203.

Kim, J., Park, B., Son, Y., & Khim, J. (2018). Peat moss-derived biochar for sonocatalytic applications. *Ultrasonics Sonochemistry, 42*, 26-30.

Lasheen, M. R., El-Sherif, I. Y., Sabry, D. Y., El-Wakeel, S. T., & El-Shahat, M. F. (2016). Adsorption of heavy metals from aqueous solution by magnetite nanoparticles and magnetite-kaolinite nanocomposite: equilibrium, isotherm and kinetic study. *Desalination and Water Treatment, 57*(37), 17421-17429.

Li, L., Liu, S. X., & Zhu, T. (2010). Application of activated carbon derived from scrap tires for adsorption of Rhodamine B. *Journal of Environmental Sciences, 22*(8), 1273-1280.

Li, Y. R., Bai, P., Yan, Y., Yan, W. F., Shi, W., & Xu, R. R. (2019). Removal of Zn2+, Pb2+, Cd2+, and Cu2+ from aqueous solution by synthetic clinoptilolite. *Microporous and Mesoporous Materials, 273*, 203-211.

Liu, C., Ngo, H. H., Guo, W. S., & Tung, K. L. (2012). Optimal conditions for preparation of banana peels, sugarcane bagasse and watermelon rind in removing copper from water. *Bioresource Technology, 119*, 349-354.

Liu, Y. C., Chen, J., Chen, M. Y., Zhang, B., Wu, D. N., & Cheng, Q. X. (2015). Adsorption characteristics and mechanism of sewage sludge-derived adsorbent for removing sulfonated methyl phenol resin in wastewater. *Rsc Advances, 5*(93), 76160-76169.

Lucian, M., & Fiori, L. (2017). Hydrothermal Carbonization of Waste Biomass: Process Design, Modeling, Energy Efficiency and Cost Analysis. *Energies, 10*(2).

Malik, P. K. (2004). Dye removal from wastewater using activated carbon developed from sawdust: adsorption equilibrium and kinetics. *Journal of Hazardous Materials, 113*(1-3), 81-88.

McEvoy, J. G., & Zhang, Z. S. (2016). Synthesis and characterization of Ag/AgBr-activated carbon composites for visible light induced photocatalytic detoxification and disinfection. *Journal of Photochemistry and Photobiology a-Chemistry, 321*, 161-170.

Meneguin, J. G., Moises, M. P., Karchiyappan, T., Faria, S. H. B., Gimenes, M. L., de Barros, M., et al. (2017). Preparation and characterization of calcium treated bentonite clay and its application for the removal of lead and cadmium ions: Adsorption and thermodynamic modeling. *Process Safety and Environmental Protection, 111*, 244-252.

Meseldzija, S., Petrovic, J., Onjia, A., Volkov-Husovic, T., Nesic, A., & Vukelic, N. (2019). Utilization of agro-industrial waste for removal of copper ions from aqueous solutions and mining-wastewater. *Journal of Industrial and Engineering Chemistry, 75*, 246-252.

Miklos, D. B., Remy, C., Jekel, M., Linden, K. G., Drewes, J. E., & Hubner, U. (2018). Evaluation of advanced oxidation processes for water and wastewater treatment - A critical review. *Water Research, 139*, 118-131.

Milenkovic, D. D., Milosavljevic, M. M., Marinkovic, A. D., Dokic, V. R., Mitrovic, J. Z., & Bojic, A. L. (2013). Removal of copper(II) ion from aqueous solution by high-porosity activated carbon. *Water Sa, 39*(4), 515-522.

Miralles, N., Valderrama, C., Casas, I., Martinez, M., & Florido, A. (2010). Cadmium and Lead Removal from Aqueous Solution by Grape Stalk Wastes: Modeling of a Fixed-Bed Column. *Journal of Chemical and Engineering Data, 55*(9), 3548-3554.

Mohammadi, S., Kargari, A., Sanaeepur, H., Abbassian, K., Najafi, A., & Mofarrah, E. (2015). Phenol removal from industrial wastewaters: a short review. *Desalination and Water Treatment, 53*(8), 2215-2234.

Mohan, D., Kumar, H., Sarswat, A., Alexandre-Franco, M., & Pittman, C. U. (2014). Cadmium and lead remediation using magnetic oak wood and oak bark fast pyrolysis bio-chars. *Chemical Engineering Journal, 236*, 513-528.

Mohapatra, D., Mishra, S., & Sutar, N. (2010). Banana and its by-product utilisation: an overview. *Journal of Scientific & Industrial Research, 69*(5), 323-329.

Monlau, F., Sambusiti, C., Antoniou, N., Zabaniotou, A., Solhy, A., & Barakat, A. (2015). Pyrochars from bioenergy residue as novel bio-adsorbents for lignocellulosic hydrolysate detoxification. *Bioresource Technology, 187*, 379-386.

Munagapati, V. S., Yarramuthi, V., Kim, Y., Lee, K. M., & Kim, D. S. (2018). Removal of anionic dyes (Reactive Black 5 and Congo Red) from aqueous solutions using Banana Peel Powder as an adsorbent. *Ecotoxicology and Environmental Safety, 148*, 601-607.

Munze, R., Hannemann, C., Orlinskiy, P., Gunold, R., Paschke, A., Foit, K., et al. (2017). Pesticides from wastewater treatment plant effluents affect invertebrate communities. *Science of the Total Environment, 599*, 387-399.

Najm, I., & Trussel, R. (1999). New and emerging drinking water treatment technologies *Identifying future drinking water contaminants* (pp. 220-260). Washington DC: The National Academic Press.

Namasivayam, C., & Kavitha, D. (2002). Removal of Congo Red from water by adsorption onto activated carbon prepared from coir pith, an agricultural solid waste. *Dyes and Pigments, 54*(1), 47-58.

Noreen, S., Bhatti, H. N., Nausheen, S., Sadaf, S., & Ashfaq, M. (2013). Batch and fixed bed adsorption study for the removal of Drimarine Black CL-B dye from aqueous solution using a lignocellulosic waste: A cost affective adsorbent. *Industrial Crops and Products, 50*, 568-579.

Oladipo, A. A., Abureesh, M. A., & Gazi, M. (2016). Bifunctional composite from spent "Cyprus coffee" for tetracycline removal and phenol degradation: Solar-Fenton process and artificial neural network. *International Journal of Biological Macromolecules, 90*, 89-99.

Oladipo, A. A., & Gazi, M. (2014). Enhanced removal of crystal violet by low cost alginate/acid activated bentonite composite beads: Optimization and modelling using non-linear regression technique. *Journal of Water Process Engineering, 2,* 43-52.

Oladipo, A. A., & Gazi, M. (2014). Fixed-bed column sorption of borate onto pomegranate seed powder-PVA beads: a response surface methodology approach. *Toxicological and Environmental Chemistry, 96*(6), 837-848.

Oladipo, A. A., & Gazi, M. (2015a). Microwaves initiated synthesis of activated carbon-based composite hydrogel for simultaneous removal of copper(II) ions and direct red 80 dye: A multi-component adsorption system. *Journal of the Taiwan Institute of Chemical Engineers, 47*, 125-136.

Oladipo, A. A., & Gazi, M. (2015b). Two-stage batch sorber design and optimization of biosorption conditions by Taguchi methodology for the removal of acid red 25 onto magnetic biomass. *Korean Journal of Chemical Engineering, 32*(9), 1864-1878.

Oladipo, A. A., & Gazi, M. (2016). Uptake of Ni2+ and rhodamine B by nano-hydroxyapatite/alginate composite beads: batch and continuous-flow systems. *Toxicological and Environmental Chemistry, 98*(2), 189-203.

Oladipo, A. A., Gazi, M., & Yilmaz, E. (2015). Single and binary adsorption of azo and anthraquinone dyes by chitosan-based hydrogel: Selectivity factor and Box-Behnken process design. *Chemical Engineering Research & Design, 104*, 264-279.

Oladipo, A. A., & Ifebajo, A. O. (2018). Highly efficient magnetic chicken bone biochar for removal of tetracycline and fluorescent dye from wastewater: Two-stage adsorber analysis. *Journal of Environmental Management, 209*, 9-16.

Oladipo, A. A., Ifebajo, A. O., & Gazi, M. (2019). Magnetic LDH-based CoO NiFe2O4 catalyst with enhanced performance and recyclability for efficient

decolorization of azo dye via Fenton-like reactions. *Applied Catalysis B-Environmental, 243*, 243-252.

Oladipo, A. A., Ahaka, E. O., & Gazi, M. (2019). High adsorptive potential of calcined magnetic biochar derived from banana peels for Cu^{2+}, Hg^{2+}, and Zn^{2+} ions removal in single and ternary systems. *Environmental Science and Pollution Research*. doi.org/10.1007/s11356-019-06321-5

Oladipo, A. A., Ahaka, E. O., & Gazi, M. (2019). Pyrochar/AgBr-derived from discarded chewing gum for decontamination of trichlorophenol via fixed-bed adsorption system. *Chemical Engineering Communications*. Manuscript submitted for publication.

Oladipo, A. A., Gazi, M., Ifebajo, A. O., Oladipo, A. S., & Ahaka, E. O. (2019). Photocatalytic degradation of toxic pesticides: Mechanistic insights. Manuscript submitted for publication.

Oladipo, A. A., Vaziri, R., & Abureesh, M. A. (2018). Highly robust AglO(3)/MIL-53 (Fe) nanohybrid composites for degradation of organophosphorus pesticides in single and binary systems: Application of artificial neural networks modelling. *Journal of the Taiwan Institute of Chemical Engineers, 83*, 133-142.

Oleiwi, H. (2014). *Treatment and reuse of produced water from Al-ahdab Iraqi oilfields*. University of Baghdad, Iraq.

Pap, S., Bezanovic, V., Radonic, J., Babic, A., Saric, S., Adamovic, D., et al. (2018). Synthesis of highly-efficient functionalized biochars from fruit industry waste biomass for the removal of chromium and lead. *Journal of Molecular Liquids, 268*, 315-325.

Papic, S., Koprivanac, N., Bozic, A. L., Vujevic, D., Dragievic, S. K., Kusic, H., et al. (2006). Advanced oxidation processes in azo dye wastewater treatment. *Water Environment Research, 78*(6), 572-579.

Patel, H. (2019). Fixed-bed column adsorption study: a comprehensive review. *Applied Water Science,* 9(3) 17pp.

Pugazhenthiran, N., Anandan, S., & Ashokkumar, M. (2016). *Removal of Heavy Metals from Wastewater* (Vol. 1). Singapore: Springer Nature.

Ramaraju, B., Reddy, P. M. K., & Subrahmanyam, C. (2014). Low Cost Adsorbents from Agricultural Waste for Removal of Dyes. *Environmental Progress & Sustainable Energy, 33*(1), 38-46.

Rao, K. S., Anand, S., & Venkateswarlu, P. (2011). Modeling the kinetics of Cd(II) adsorption on Syzygium cumini L leaf powder in a fixed bed mini column. *Journal of Industrial and Engineering Chemistry, 17*(2), 174-181.

Rashed, M. N. (2013). *Adsorption Technique for the Removal of Organic Pollutants from Water and Wastewater," in Organic Pollutants - Monitoring, Risk and Treatment*: INTECH.

Rawtani, D., Khatri, N., Tyagi, S., & Pandey, G. (2018). Nanotechnology-based recent approaches for sensing and remediation of pesticides. *Journal of Environmental Management, 206*, 749-762.

Redah, M. A. (2016). Wastewater treatment using successive electrochemical approaches (Unpublished doctoral dissertation). University of Baghdad , Republic of Iraq.

Reungoat, J., Escher, B. I., Macova, M., Argaud, F. X., Gernjak, W., & Keller, J. (2012). Ozonation and biological activated carbon filtration of wastewater treatment plant effluents. *Water Research, 46*(3), 863-872.

Riazi, M., Keshtkar, A. R., & Moosavian, M. A. (2016). Biosorption of Th(IV) in a fixed-bed column by Ca-pretreated *Cystoseira indica*. *Journal of Environmental chemical Engineering 4*(2), 1890-1898.

Rong, X., Xie, M., Kong, L. S., Natarajan, V., Ma, L., & Zhan, J. H. (2019). The magnetic biochar derived from banana peels as a persulfate activator for organic contaminants degradation. *Chemical Engineering Journal, 372*, 294-303.

Rossini, M., Garrido, J. G., & Galluzzo, M. (1999). Optimization of the coagulation-flocculation treatment: Influence of rapid mix parameters. *Water Research, 33*(8), 1817-1826.

Rouf, S., & Nagapadma, M. (2015). Modeling of Fixed Bed Column Studies for Adsorption of Azo Dye on Chitosan Impregnatedwith a Cationic Surfactant. *International Journal of Scientific & Engineering Research, 6*(2), 538-545.

Selvanathan, M., Yann, K. T., Chung, C. H., Selvarajoo, A., Arumugasamy, S. K., & Sethu, V. (2017). Adsorption of Copper(II) Ion from Aqueous Solution Using Biochar Derived from Rambutan (Nepheliumlappaceum) Peel: Feedforward Neural Network Modelling Study. *Water Air and Soil Pollution, 228*(8) 1-19.

Serafin, J., Narkiewicz, U., Morawski, A. W., Wrobel, R. J., & Michalkiewicz, B. (2017). Highly microporous activated carbons from biomass for CO2 capture and effective micropores at different conditions. *Journal of Co2 Utilization, 18*, 73-79.

Shah, M. P., Reddy, G. V., Banerjee, R., Babu, P. R., & Kothari, I. L. (2005). Microbial degradation of banana waste under solid state bioprocessing using two lignocellulolytic fungi (Phylosticta spp. MPS-001 and Aspergillus spp. MPS-002). *Process Biochemistry, 40*(1), 445-451.

Sher, F., Malik, A., & Liu, H. (2013). Industrial polymer effluent treatment by chemical coagulation and flocculation. *Journal of Environmental Chemical Engineering, 1*, 684-689.

Silva, A., Stawinski, W., Romacho, J., Santos, L., Figueiredo, S. A., Freitas, O. M., et al. (2019). Adsorption of Fluoxetine and Venlafaxine onto the Marine

Seaweed Bifurcaria bifurcata. *Environmental Engineering Science, 36*(5), 573-582.

Singh, K., & Arora, S. (2011). Removal of Synthetic Textile Dyes From Wastewaters: A Critical Review on Present Treatment Technologies. *Critical Reviews in Environmental Science and Technology, 41*(9), 807-878.

Sivarajasekar, N., Balasubramani, K., Mohanraj, N., Maran, J. P., Sivamani, S., Koya, P. A., et al. (2017). Fixed-bed adsorption of atrazine onto microwave irradiated Aegle marmelos Correa fruit shell: Statistical optimization, process design and breakthrough modeling. *Journal of Molecular Liquids, 241*, 823-830.

Sizmur, T., Fresno, T., Akgul, G., Frost, H., & Moreno-Jimenez, E. (2017). Biochar modification to enhance sorption of inorganics from water. *Bioresource Technology, 246*, 34-47.

Sun, H. Y., Sun, L. P., Li, F., & Zhang, L. (2015). Adsorption of benzothiophene from fuels on modified NaY zeolites. *Fuel Processing Technology, 134*, 284-289.

Sweetman, M. J., May, S., Mebberson, N., Pendleton, P., Vasilev, K., Plush, S. E., et al. (2017). Activated carbon, carbon nanotubes and graphene: Materials and composites for advanced water purification. *Journal of Carbon Research, 3*(18), 1-29.

Tanyildizi, M. S. (2011). Modeling of adsorption isotherms and kinetics of reactive dye from aqueous solution by peanut hull. *Chemical Engineering Journal, 168*(3), 1234-1240.

Tran, H. N., Lee, C. K., Vu, M. T., & Chao, H. P. (2017). Removal of Copper, Lead, Methylene Green 5, and Acid Red 1 by Saccharide-Derived Spherical Biochar Prepared at Low Calcination Temperatures: Adsorption Kinetics, Isotherms, and Thermodynamics. *Water Air and Soil Pollution, 228*(10), 1-16.

Tran, N. H., Chen, H. J., Reinhard, M., Mao, F., & Gin, K. Y. H. (2016). Occurrence and removal of multiple classes of antibiotics and antimicrobial agents in biological wastewater treatment processes. *Water Research, 104*, 461-472.

Tripathi, N. K., Singh, V. V., Sathe, M., Thakare, V. B., & Singh, B. (2018). Activated Carbon Fabric: An Adsorbent Material for Chemical Protective Clothing. *Defence Science Journal, 68*(1), 83-90.

Villegas, L. G. C., Mashhadi, N., Chen, M., Mukherjee, D., Taylor, K. E., & Biswas, N. (2016). A Short Review of Techniques for Phenol Removal from Wastewater. *Current Pollution Reports, 2*(3), 157-167.

Wajima, T. (2017). A new carbonaceous adsorbent for heavy metal removal from aqueous solution prepared from paper sludge by sulfur-impregnation and pyrolysis. *Process Safety and Environmental Protection, 112*, 342-352.

Wang, J. L., & Xu, L. J. (2012). Advanced Oxidation Processes for Wastewater Treatment: Formation of Hydroxyl Radical and Application. *Critical Reviews in Environmental Science and Technology, 42*(3), 251-325.

Wang, T., Wu, J. W., Zhang, Y. S., Liu, J., Sui, Z. F., Zhang, H. C., et al. (2018). Increasing the chlorine active sites in the micropores of biochar for improved mercury adsorption. *Fuel, 229*, 60-67.

Wang, Z. Y., Liu, G. C., Zheng, H., Li, F. M., Ngo, H. H., Guo, W. S., et al. (2015). Investigating the mechanisms of biochar's removal of lead from solution. *Bioresource Technology, 177*, 308-317.

Yakout, S. M., & El-Deen, G. S. (2016). Characterization of activated carbon prepared by phosphoric acid activation of olive stones. *Arabian Journal of Chemistry, 9*, S1155-S1162.

Yan, Y. K., Xiang, B., Yi, X. W., Li, Y. J., & Jia, Q. (2014). Competitive Adsorption of Acid Dyes from Aqueous Solution on Diethylenetriamine-Modified Chitosan Beads. *Journal of Applied Polymer Science, 131*(23), 1-9.

You, Z. Y., Zhuang, C., Sun, Y. J., Zhang, S. J., & Zheng, H. L. (2019). Efficient Removal of TiO2 Nanoparticles by Enhanced Flocculation-Coagulation. *Industrial & Engineering Chemistry Research, 58*(31), 14528-14537.

Yu, D. Y., Wang, L. L., & Wu, M. H. (2018). Simultaneous removal of dye and heavy metal by banana peels derived hierarchically porous carbons. *Journal of the Taiwan Institute of Chemical Engineers, 93*, 543-553.

Zaghouane-Boudiaf, H., & Boutahala, M. (2011). Adsorption of 2,4,5-trichlorophenol by organo-montmorillonites from aqueous solutions: Kinetics and equilibrium studies. *Chemical Engineering Journal, 170*(1), 120-126.

Zango, Z. U., Garba, Z. N., Abu Bakar, N. H. H., Tan, W. L., & Abu Bakar, M. (2016). Adsorption studies of Cu2+-Hal nanocomposites for the removal of 2,4,6-trichlorophenol. *Applied Clay Science, 132*, 68-78.

Zhong, L. C., Zhang, Y. S., Ji, Y., Norris, P., & Pan, W. P. (2016). Synthesis of activated carbon from coal pitch for mercury removal in coal-fired power plants. *Journal of Thermal Analysis and Calorimetry, 123*(1), 851-860.

Zhou, N., Chen, H. G., Xi, J. T., Yao, D. H., Zhou, Z., Tian, Y., et al. (2017). Biochars with excellent Pb(II) adsorption property produced from fresh and dehydrated banana peels via hydrothermal carbonization. *Bioresource Technology, 232*, 204-210.

Zhu, Y. F., Wang, W. B., Zhang, H. F., Ye, X. S., Wub, Z. J., & Wang, A. Q. (2017). Fast and high-capacity adsorption of Rb+ and Cs+ onto recyclable magnetic porous spheres. *Chemical Engineering Journal, 327*, 982-991.